Appendix to

Reconstructing the Alps-Carpathians-Dinarides as a key to understanding switches in subduction polarity, slab gaps and surface motion

Mark R. Handy[1], Kamil Ustaszewski[1, 2], Eduard Kissling[3]

[1] Freie Universität Berlin, D-12249 Berlin, Germany

[2] Friedrich-Schiller-Universität Jena, D-07749 Jena, Germany

[3] Eidgenössische Technische Hochschule (ETH), CH-8092 Zürich, Switzerland

Contents

A. Restoring the Apennines-Alps-Carpathians-Dinarides (ApAlCaDi) orogenic system and constructing paleotectonic maps for 20 Ma, 35 Ma, 67 Ma and 84 Ma

A1. Projection and General Approach

The paleotectonic maps in **Figures 5, 6, 8 and 10** were constructed in a Lambert Conformal Conic projection with a central meridian at 16°E. Their construction entailed restoring the main tectonic units in the Alps (Fig. **A1**) to their positions in the past, then positioning the local structures between these restored units based on geological information and arguments.

Faults that appear as discrete structures (lines) on the map scale in Figure **A1** and Figure **2** of the main text are in reality zones of distributed deformation some hundreds of meters wide that affect units in both their hanging- and footwalls. Because major faults often truncate several different units in their footwalls, we define (and name) major faults in our reconstructions according to the tectonic units in their hangingwalls, as listed in Table **A1**. Sutures which have been reactivated as faults are named after the ocean basin from which the ophiolites are derived.

A2. Restoration Procedure

To restore the tectonic units to past locations, we first identify the main faults in the Alps (Fig. **A2,** Table **A1**) then simplify their geometry by subdividing them into straight-line segments (Fig. **A3**). Faults chosen as markers (Fig. **A2**) include the following thrust fronts and other major structures: (1) the trailing edge of the Jura thrust-and-fold belt; (2) the thrust front of the deformed foredeep of the Alps (Subalpine Molasse) onto Plateau Molasse of the less- to undeformed foredeep; (3) the thrust front of the Helvetic nappes and the Châines Subalpines; (4) the thrust front of the Maritime Alps; (5) the thrust front of the Penninic units (i.e., Penninic Front or Roselend Thrust of Ceriani et al. 2001), following the sutured remains of the Cretaceous Valais Ocean; (6) the thrust front of the Piemont-Liguria Suture in the Western Alps which includes ophiolites of the Early Jurassic Piemont-Liguria Ocean; (7) the main branch of the Periadriatic Fault System. These faults were chosen because they delimit the main Mesozoic paleogeographic units and have good biostratigraphic and radiometric age constraints for tracking displacement.

The Molasse basin extends to the southwest to just northeast of Lyon (Fig. **2** in the text); the Subalpine Molasse Front merges along strike with the front of the Châines Subalpines in the Chablais area (Faults 2 and 3 in Figs. **A2** and **A3**). Faults 5 and 6 are separated by nappes derived from the Briançonnais continental sliver, which is variously interpreted as the easternmost tip of the Iberian Plate (e.g., Stampfli and Borel 2002) or an elongate, sliver-like extensional allochthon that rifted off of the European margin in Early Cretaceous time (e.g., Handy et al. 2010). Whatever their origin, Briançonnais-derived units can be followed eastward only as far as the Engadine Window (Fig. **A1**). There, the Valais and Piemont-Liguria sutures of Alpine Tethys (i.e., Faults 5 and 6) join, but can still be differentiated on lithological grounds (Schmid et al. 2008, 2013) and continue eastward into the Tauern Window (Fig. **A1**). The front of these sutures runs as a composite thrust along the northern margin of the Eastern Alps, just south of Fault 3, i.e., structurally above the Helvetic Nappes and below the

Austroalpine units. To prevent cluttering of our figures, we do not show the eastern composite trace of Faults 5 and 6 in Figure **A3**.

The tectonic units bounded by the fault systems above are restored in a series of rigid-body motions with respect to autochthonous Variscan basement of the stable European foreland located east of the Cenozoic Rhine-Bresse Graben system (Black Forest Mts. Marked in Figs. **A2** and **A3**). The restoration proceeded stepwise from external to internal parts of the Alpine chain, with shortening values from published maps and cross sections (references in caption to Fig. **A1**) applied as successive retrotranslations to the Adriatic Plate. For reasons outlined below and in the main text, the city of Ivrea within the arc of the Western Alps (location marked with an **I** next to a small cross on all figures) was chosen to be the reference point on the stable part of the Adriatic Plate.

The displacements are obtained from cross sections by measuring the distance between corresponding contacts in the foot- and hangingwalls of faults. Displacements obtained in this way must be regarded as minimum estimates of the true displacement because the cut-off lines for the contacts are either eroded along the thrust fronts or are buried beneath overlying thrust sheets. Furthermore, we cannot exclude the possibility that tectonic erosion removed previously accreted units from along the orogenic front. The same caveat applies to shortening estimates obtained from 2-D, map-view displacement fields.

The stepwise nature of restoration reflects the geometric need to discretize motions that in nature were actually continuous and, in some cases, even coeval. This pertains especially to the restoration of Insubric and Helvetic deformations in the Western Alps in step 6 below. During each step back in time, we maintain a best fit of the fault segments with the directions and lengths of published shortening for those segments. This involves manually adjusting the fit of the fault segments during each step in order to to avoid any shortening that is less than the published shortening estimate for the same segments and time interval. However, we allow the shortening during restoration to exceed published displacements for a given segment, which must be regarded as minimum estimates for the reasons discussed above.

We adopt the restoration of Ustaszewski et al. (2008) of the Carpathians for 20 Ma which accounts for Miocene shortening in the Carpathians and extension in the Pannonian Basin. The restoration of the Apennines is taken from the paleotectonic maps of Handy et al. (2010) as modified from Rosenbaum et al. (2002) and Viti et al. (2009). The Dinarides are the least constrained part of our reconstruction, primarily due to incomplete knowledge of the amount of shortening and the age of the major faults.

A3. Map reconstruction at 20 Ma (Fig. 10 in the main text)

A3.1 Restoring the Jura fold-and-thrust belt (step 1, Fig. **A4**)

We restore the trailing edge of the Jura thrust-and-fold belt (Fault 1) using 2-D displacement fields (Philippe et al. 1996). These indicate a variable amount of Neogene shortening along strike of the belt, from a maximum of 39 km at the southwest end of the belt to 0 km in the northeast near Zürich (Fig. **A1a**). Restoration of the Jura leads to straightening of the more internal fault segments in the Central Alps and to retrotranslation of the other faults in the Western Alps. Deformation in the Jura Mountains lasted from about 13 Ma to 5 Ma (Becker 2000, Ustaszewski and Schmid 2006) and affected primarily detached Mesozoic cover sediments of the European

basement. There are indications that thrusting also involved this basement since Late Pliocene time and indeed, may still be ongoing (Ustaszewski and Schmid 2007a, Schmid and Slejko 2009, Madritsch et al. 2008). However, the thick-skinned component of deformation is negligible and therefore not included in our reconstruction. The same applies to the Alpine foredeep, which shows only minor deformation of the Plateau Molasse (e.g., Pfiffner 1986, Burkhard 1990). The decollement of the Jura Mountains is linked beneath the Molasse Basin to the basal thrust of the External Basement Massifs (Pfiffner 1986, Schmid et al. 1996, Burkhard and Sommaruga 1998), so that we do not incorporate shortening of these massifs separately in steps 1 to 6. In addition, there is an unknown amount of shortening of the Oligo-Miocene sediments of the Molasse Basin (Pfiffner 1986, Jon Mosar, personal communication, 2013) which are also not accounted for in this step due to the poor time constraints on subsurface structures.

A3.2 Restoring the Subalpine Molasse Front and Châines Subalpines (step 2, Fig. **A5**)

Most thrusting and folding of the Subalpine Molasse (Fault 2) occurred between about 23 Ma and 5 Ma (Burkhard 1990, Schlunegger et al. 1997, Ortner et al. 2011, von Hagke et al. 2012). The amount of Neogene shortening perpendicular to the strike of the Alps varies along the strike of faults 2 and 3 (Fig. **A1a**) from a maximum of 36 km in the Central Alps to about 10 km and even less to the east and south. Shortening in the Penninic units is also minor (11 km) and, if our reconstruction is valid, may be related to Neogene sinistral strike-slip motion. The External Basement Massifs (light blue units with crosses in Fig. **A1a**) were exhumed along steep, out-of-sequence thrusts throughout Miocene time (e.g., 22 to 6 Ma for the Mont Blanc Massif, Leloup et al. 2005). The amount of shortening along the basal thrusts of these Massifs is modest compared to their impressive topographic relief of 2000-4000m. In the Aar Massif, for example, N-directed shortening amounts to about 21 km, of which 15 km occurred in mid- to late Miocene time (Schmid et al. 1996, their table 1). For practical reasons related to the out-of-sequence nature of this thrusting, we have neglected this minor shortening in our reconstruction.

A3.3 Restoring the Maritime Alps Front (step 3, Fig. **A6**)

Post-20 Ma shortening along the Maritime Alpes Front amounted to 11-14 km. Due to the rigid-body translations involved in retrodeformation, this modest displacement in the Maritimes Alpes yields about 26-36 km of predicted Miocene shortening along the Penninic Front (Fig. **A6**). This amount may be kinematically linked to some 30 km of post-20 Ma dextral motion along the Periadriatic Fault System (Fig. **A1a**) related to E-W extension of the Lepontine Dome across the Simplon Fault (Graseman and Mancktelow 1993). However, most displacement along the Periadriatic Fault System accrued between 34 and 20 Ma, during northwestward Adriatic indentation of the Western Alps (i.e., during the second deformation phase of Ceriani and Schmid 2004).

A3.4 Restoring Giudicarie strike-slip faulting and Penninic N-S shortening in the Central and Eastern Alps (step 4, Fig. **A7**)

This restoration involves two substeps: First, sinistral motion along the Giudicarie Fault is retrodeformed to yield a nearly straight Periadriatic Fault, then this straightened fault is restored to a position that is compatible with Miocene north-south directed shortening in the Eastern Alps. The rationale behind these substeps is outlined in the two substeps below.

A3.4.1 Age and displacement of the Giudicarie Fault (substep 4-1)

The Giudicarie Fault offsets the Periadriatic Fault by some 80 km (Fig. **A1a,** e.g., Laubscher 1971, Pomella et al. 2011, 2012). The Periadriatic Fault accommodated dextral strike-slip motion from Oligocene to Early Miocene time (e.g., Schmid et al. 1989) and clearly pre-dates the Giudicarie Fault. Biostratigraphic markers in sediments both above and below Giudicarie-related thrusts in the Southern Alps indicate that the main phase of Giudicarie faulting initiated no later than 20-23 Ma (Luciani and Silvestrini 1996, Scharf et al. 2013, Schmid et al. 2013) and continued to mid-Miocene time at about 10 Ma (Rosenberg and Berger 2009). Giudicarie faulting ended no later than 7 Ma, as constrained by the age of the Messinian unconformity that seals the Milan thrust forming the lateral continuation of the Giudicarie Fault (Pieri and Groppi 1981). The sinistral offset along the Giudicarie Fault is not transferred to the northern thrust front of the Alps, but was instead accommodated in the Eastern Alps by a combination of doming, E-W orogen-parallel stretching and erosion in the Tauern Window (Scharf et al. 2013). Retrodeforming the Giudicarie Fault by 80 km restores the Periadriatic Fault to an almost straight line with only a minor jog remaining in the vicinity of the Giudicarie Fault (Fig. **A1**). This jog may have been an inherited paleogeographic feature (e.g., early Mesozoic normal fault, Doglioni and Bosellini 1987, Viola et al. 2001, Castellarin et al. 2006) that was reactivated during Alpine convergence.

A3.4.2 Post-20 Ma shortening of the Eastern Alps (substep 4-2)

Post-20 Ma north-south shortening of the Eastern Alps in the vicinity of the Tauern Window varies from about 86 to 113 km according to the 2-D displacement field of Linzer et al. (2002) shown in Figure **A1a**. This range must be considered a minimum estimate because the authors tacitly assume that Miocene shortening across the Tauern Window was accommodated only by orogen-parallel extension along normal faults and conjugate strike-slip faults, with little or no contribution of upright folding and erosion to Miocene exhumation of the Penninic units in the Tauern Window (Schneider et al., submitted). If 100 km is taken as a reasonable average of Miocene north-south shortening in this part of the Eastern Alps (Fig. **A7**), then no more than 50-70 km of this total is due to northward motion of the eastern Adriatic indenter along the sinistral Giudicarie Fault. This leaves 30-50 km of Miocene shortening within the Penninic domain, a value which is consistent with an estimated 30-49 km of N-S shortening due to upright, post-nappe folding in the western part of the Tauern Window (respectively, Schmid et al. 2013 and Rosenberg and Berger 2009).

Accommodating 100 km of post-20 Ma N-S shortening in the Eastern Alps while allowing for only minor Miocene N-S shortening of internal Penninic units of the Western Alps requires bending the Periadriatic Fault in the vicinity of its intersection

with the northern end of the future Giudicarie Fault. This bending rotates and restores the western segment of the Periadriatic Fault into its present orientation with respect to the eastern segment, as shown for the final trace of this fault in Figure **A7**. This operation calls for about 50 km of Miocene N-S shortening in the Central Alps, only 9 km more than the 41 km of Miocene shortening recently proposed for the Central Alps by Rosenberg and Kissling (2013, their fig. 3b) along the NFP-20E transect.

A3.5 Restoring the Southern Alps Front, backrotating the Adriatic Plate (step 5, Fig. **A8**)

The backrotation of the Adriatic Plate with respect to Europe is constrained first by the choice of a vertical pole of rotation at the city of Ivrea, and second by the overall eastward increase in Miocene, S-directed shortening in the Southern Alps (Fig. **A8**). Ivrea is an appropriate site for the Adriatic rotational pole for the following reasons: (1) Ivrea is located within the Ivrea crustal cross section (Fig. **A1**), an upended piece of the Mesozoic continental margin of Adria that escaped penetrative Alpine deformation (e.g., Zingg et al. 1990); (2) Ivrea generally coincides with rotational poles for Adria derived from a plate kinematic reconstruction of the Carpathians and Dinarides at 20 Ma (Ustaszewski et al. 2008) as well as from geodetic data for present-day plate motion (seismic moment: Anderson and Jackson 1987; Very long baseline interferometry, VLBI: Ward 1994; GPS: e.g., Calais et al. 2002, Vrabec et al. 2006).

A rotational angle of 20° about Ivrea is obtained by drawing lines from Ivrea to the end and tip of the 72 km shortening vector in the western part of the Southern Alps (Fig. **A8**, Schönborn 1992). This angle is very sensitive to the amount of shortening in the Southern Alps and to the distance of this shortening vector from the rotational pole at Ivrea. Indeed, smaller (16°) rotations result if one uses the displacement vectors associated with 50 km of S-directed thrusting in the Dolomites (Schönborn 1999) and the Friuli part of the Southern Alps (Fig. **A1a;** Nussbaum 2000). However, the 20° rotation is consistent with an estimated 300 km of post-Eocene shortening in the central Dinarides at the latitude of Dubrovnik (39°N, Schefer et al. 2011, p. 1200 based on Schmid et al. 2008) some 850 km away from Ivrea (Fig. **6**). The timing of this rotation is bracketed by stratigraphic controls on the age of thrusting in the Southern Alps (20-7 Ma, Pieri and Groppi 1981, Schönborn 1992) and by paleomagnetic data showing that 20-25° rotation affected Eocene and Oligocene sediments of the stable Adriatic platform (Marton et al. 2010, 2011). Better constraints are unavailable, primarily due to the paucity of Miocene sediments (Schönborn 1992, Schumacher et al. 1996).

A3.6 Restoring the Carpathians, Dinarides and Hellenides at 20 Ma

The Carpathians at the onset of rollback subduction at 20 Ma are reconstructed by restoring back-arc extension in the AlCaPa (290 km) and Tisza-Dacia (180 km) units of the Pannonian Basin (Ustaszewski et al. 2008). Expansion of the orogenic arc into the Carpathian Embayment of Alpine Tethys was associated with many smaller crustal scale block rotations, as discussed in Ustaszewski et al. (2008, their fig. 6). These are not shown in Figure **10**. The orogenic front of the Western Carpathians at 20 Ma is the flysch front in the foredeep of the Carpathian orogen (Ustaszewski et al. 2008) and joins laterally to the west with the restored position of the Helvetic front.

The Mid-Hungarian Fault Zone is a key structure insomuch it accommodated differential eastward motion and extension of the AlCaPa and Tisza-Dacia blocks in the upper plate of the Carpathian rollback subduction in Miocene time (e.g., Fodor et al.

1998, Horváth et al. 2006; Ustaszewski et al. 2008). The Mid-Hungarian Fault Zone comprises several fault strands that are buried beneath the Pannonian plain. Its southern limit is the so-called Mid-Hungarian Line (Csontos and Nagymarosy 1998) or Zagreb-Tremplin Line (Haas 2001) which skirts the northern boundary of the Tisza Unit (Figs. **2** and **10**). Its northern limit is the Balaton Fault (Fig. **2**) which is the eastern continuation of the Periadriatic Fault.

We emphasize that the Mid-Hungarian Fault Zone did not link the Alpine and Dinaric orogenic fronts and was therefore not a trench-trench transfer fault like the ADT1 and ADT2. Instead, it accommodated differential extension and vertical block rotations in the upper plate of the retreating Carpathian orogen, and overprinted the latter faults as shown in Figure **10**. We speculate that at 20 Ma the southwestern end of the Mid-Hungarian Fault Zone was continuous with the ADT2, which had ceased to be active as a transfer fault when Adria-Europe convergence in the Alps began to be taken up along the Southern Alps Front.

The location and orientation of main faults in the Dinarides at 20 Ma (Fig. **10**) is based on the maps of Horváth et al. (2006), Schmid et al. (2008) and the reconstruction of Ustaszewski et al. (2008, their fig. 6). In the central and southern Dinarides, the orientation of these faults with respect to Europe is interpreted to have remained constant from the present time back to 20 Ma (compare Figs. **2** and **10**). This is based on paleomagnetic evidence from Oligocene to Mio-Pliocene Dinaric Lake System sediments (de Leeuw et al. 2012) that the main Dinaric faults and fault blocks have not rotated since deposition.

Faults in the northern Dinarides that accommodated Miocene shortening are difficult to identify, especially because the ages of flysch in the footwalls of thrusts are controversial. Most workers favour Paleogene depositional ages based on detrital nannoplankton (e.g., Babić et al. 2007), but others (Mikes et al. 2008 and references therein) claim to have found Miocene nannofossils in flysch of the External Dinarides. In this paper, we opt for the conservative interpretation of late Paleogene flysch ages in most of the External Dinarides. This necessitates that Neogene Adria-Europe convergence was accommodated by reactivated fold-and-thrust systems in the External Dinarides or possibly even in the Internal Dinarides. For kinematic simplicity, we link the Southern Alps Front with the Miocene Dinaric deformation front via the dextrally transpressive Split-Karlovac Fault (SK in Fig. **10**, Chorowicz 1970, 1975). This fault is a good candidate to link these fronts because it cross-cuts the Dinaric thrusts and was active in Miocene time as evidenced by early-middle Miocene lacustrine deposits that are pinched in along the fault (Polšak et al. 1976; Šušnar and Bukovac 1978, 1:100,000 sheets “Bihać” and “Drvar” of the Geological Map of Yugoslavia). According to these maps, the Split-Karlovac Fault splays into thrusts, some of which offset, and others which merge with, and thefore reactivate late Paleogene thrusts.

In the northernmost Dinarides, i.e., in northern Slovenia and northern Croatia, north-south shortening and clockwise block rotations related to Miocene indentation and dextral motion along the Periadriatic Fault substantially modified the orientation of pre-Neogene faults, including the ADT2. Tomljenović et al. (2008) present paleomagnetic evidence from the Medvednica Mountains area near Zagreb (location in Fig. **1**, Me in Fig. **10**) that documents clockwise block rotations of up to 130°. These rotations reoriented originally NW-SE trending Dinaric thrusts into their present ENE-WSW to E-W orientation. The authors argue that most of this clockwise rotation occurred in late Paleogene, probably latest Oligocene to early Miocene time.

The geometry of the Hellenides southeast of the Scutari-Peç Fault (SP) at 20 Ma is obtained by interpolating the locations of paleogeographic units in the Aegean

reconstructions for 25 Ma and 15 Ma of van Hinsbergen and Schmid (2012, their figs. 11b, c). In contrast to the Dinarides, the northwestern Hellenides have undergone up to 40-60° of clockwise rotation with respect to Europe during rollback subduction since late Oligocene time (e.g., Broadley et al. 2006). A substantial part of this rotation has occurred since 20 Ma (Kissel and Laj 1988, van Hinsbergen et al. 2005) and continues at present (e.g., Jouanne et al. 2012). The rotation pole for this clockwise rotation is situated at or near the SP (Kissel and Laj 1988, van Hinsbergen et al. 2005) which is interpreted to be the NW limit of Aegean back-arc extension (Kissel et al. 1995). To restore this extension in Figures **5** and **6**, we use the reconstructions of Burchfiel et al. (2008, their figs. 5-10) which document a change from N-S to NE-SW directed extension during late Paleogene to Holocene time between the Fore-Balkan fold-and-thrust belt (FB in Fig. **10**) and the southwestern part of the Hellenic Front.

A3.7 Summary of Adriatic Plate motion since 20 Ma

Restoring all known post-20 Ma shortening in the Alps in steps 1-5 results in a displacement of the Adriatic Plate some 113 km to the NW (325°) at the city of Ivrea (Figs. **A9 and 10**). This vector can be broken down into a westward component of 59 km and a northward component of 92 km. In addition, the Adriatic Plate rotated CCW by some 20° around Ivrea with respect to the stable European foreland (Fig. **A9**).

In light of the modest amounts of post-20 Ma shortening across various parts of the Western Alpine arc (several tens of km**,** Fig. **A1a**), the estimated 113 km of NW-SE directed Adria-Europe convergence at Ivrea seems too high, even though this estimate does not include the 15-21 km of Neogene shortening related to out-of-sequence thrusting in the External Basement Massifs (section A3.2). However, it can be argued that this amount is roughly consistent with approximately 100 km of post-20 Ma subduction obtained by subtracting 200 km of 20-35 Ma shortening in the NW-SE direction of convergence (A4.5) from the maximum 300 km length of the ruptured European slab imaged in the ECORS-CROP section (Lippitsch et al. 2003, their fig. 13a, Kissling et al. 2006, their fig. 14a).

When assessing the validity of the 113 km displacement vector, it is important to note that this estimate is obtained by retrotranslating all post-20 Ma thrust fronts in a direction perpendicular to their various trends around the arc of the Western Alps. This procedure creates a space problem within the arc that is only resolved when the point at Ivrea is allowed to move freely along the resultant of the displacement vectors of the faults. The resultant vector exceeds the sum of the displacements on the individual faults, which are assumed not to rotate in map view during thrusting; backrotations of the faults about vertical rotation axes are carried out in a separate step during straightening of the Western Alps (step 7 below, section A4.2). This discretized approach to retrodeforming the Western Alps also affects the azimuth of Adriatic motion, although the effect is difficult to quantify. Thus, we emphasize that the 113 km estimate is an upper bound on the amount of post-20 Ma NW-SE–directed Adria-Europe convergence. Nevertheless, we use it in order to maintain a consistent approach in all steps of the reconstruction.

A4. Map reconstruction at 35 Ma (Fig. 8 in the main text)

In the Alps, 35 Ma marks the incipient transition from oceanic subduction and the deposition of orogenic flysch-type trench sediments to continental collision and the formation of a flexural foredeep with Molasse-type sedimentation (e.g., Schmid et al. 1996, Handy et al. 2010). This time is also when Adria-Europe convergence slowed and changed direction (e.g., Handy et al. 2010), triggering slab breakoff and calc-alkaline magmatism in the Alps and Dinarides (Fig. **3** in the main text). The map in Figure **8** of the main text was constructed according to steps 6 and 7 below and uses the estimates of late Paleogene shortening compiled in Figure **A1b**.

A4.1 Restoring Helvetic, internal Penninic and Insubric deformations (step 6)

The so-called Insubric phase of deformation (Argand 1916) lasted from c. 35 to 20 Ma and affected primarily the previously subducted and exhumed Paleogene nappes in the core of the Alps and along the Periadriatic Fault System, or PFS (Schmid et al. 1989). This prominent tectonic lineament has a long history beginning with Mesozoic transform activity during the oblique opening of Alpine Tethys (Schmid et al. 1989; Handy et al. 2010). For the purposes of our reconstruction, we focus on its Cenozoic kinematics and the related emplacement of the Penninic and Helvetic Nappes.

A4.1.1 The Helvetic Nappes

The Helvetic Nappes were emplaced onto the European foreland during late Paleogene to early Miocene time, i.e., at 34-22 Ma (Schmid et al. 1996, their fig. 4). Our restoration uses Pfiffner's estimates of the total amount of Cenozoic shortening in the Helvetic nappes (Pfiffner 2009, pp. 233-235, his fig. 5.2-14), except that we neglect minor shortening associated with out-of-sequence thrusting of the External Basement Massifs in late Miocene time (6 km of N-S shortening along the NFP20E section according to Schmid et al. 1996, their table 1). The Helvetic Nappes are restored southwards by an amount that decreases going from NE to SW along the thrust front (Figs. **A1b, A10,** Kempf and Pfiffner 2004).

In the absence of published shortening estimates for the Helvetic Nappes in the Eastern Alps, we simply assume that shortening there was the same as in the NFP20E section (Fig. **A10**). This is quantitatively unconstrained but qualitatively consistent with evidence of Paleogene shortening in the Austroalpine units (28-23 Ma, Linzer et al. 2002) and avoids space problems in the Dinarides that would arise if less N-S Paleogene shortening in the Eastern Alps had to be compensated by an equivalent amount of younger N-S shortening of internal Dinaric units (e.g., along the Sava suture zone), for which there is no evidence so far.

A4.1.2 Internal Penninic deformation

Insubric shortening of the internal Penninic units in the Western Alps (i.e., the units between the Periadriatic Fault and the Penninic Front) amounted to about 40 km (**Fig. A10**) as estimated from the kinematic reconstruction of Ford et al. (2006). We obtained this value from their paleotectonic maps for 34-37 Ma and 15-17 Ma (their figs.

5b, d) by measuring the decrease in orogen-perpendicular distance between the Penninic Front (Roselend Thrust of Ceriani et al. 2001) and the western branch of the Periadriatic Fault System (Canavese Line) which delimits the Ivrea Zone.

A4.1.3 Late Paleogene Insubric strike-slip motion

We translated the Periadriatic Fault and the Adriatic Plate 150 km to the east (90°) with respect to Europe (Fig. **A1b**). This distance corresponds to the dextral offset of distal Adriatic units in the Central and Western Alps (i.e., Lower Austroalpine Sesia-Dent Blanche and Margna units, Laubscher 1991) and represents the total amount of east-west Insubric shortening between the Periadriatic Fault and the external front of the Western Alps (Fig. **A10**). 150 km of shortening is roughly compatible with the minimum 170-180 km length of the broken part of the east-dipping slab anomaly beneath the Western Alps as imaged by tomography along the ECORPS-CROP transect (Lippitsch et al. 2003, their fig. 13a) and discussed in section 3.3 of the main text. We trust the conservative estimate of 150 km because restoring the Southern Alps any further to the east would leave too little space between the Dinarides and the Moesian promontory of stable Europe (see Fig. **8** in the text). Any more than 150 km of E-W Insubric strike-slip displacement would require significant Neogene east-west extension of Internal Dinaric and accreted European units instead of the observed Eocene to early Miocene dextral transpressional tectonics just west of the Moesian promontory of Europe. This transpression was associated with the lateral northeastward extrusion of the amalgamated Tisza and Dacia units into the space that opened behind the expanding Carpathian Arc in Miocene time and that is presently occupied by the Pannonian Basin (Fügenschuh and Schmid 2005, their figs. 9c, d).

A4.2 Unfolding the arc of the Western Alps (step 7)

Our attempt to unfold the arc of the Western Alps begins with three basic observations: (1) The Western Alps and northern Apennines show opposite senses of curvature in map view (Fig. **2**) as well as opposite directions of subduction as imaged in travel-time seismic tomography (e.g., Piromallo and Morelli 2003, Spakman and Wortel 2004): subduction is to the east beneath the Western Alps (Kissling et al. 2006) and to the west beneath the northern Apennines (see also Zhu et al. 2012, section Cc in their fig. 3); (2) Paleomagnetic work indicates that internal units of the Western Alps have undergone significant counterclockwise (CCW) rotations relative to Europe since Oligocene time (Thomas et al. 1999, Collombet et al. 2002), but not external units which experienced little, if any, rotation (Aubourg and Chabert-Pelline 1999). Moreover, the amount of rotation in the internal units increases to the south from the Briançonnais and Umbaye parts to the Ligurian part of the Western Alps (47-117 ° for segments d, e, f of faults 3 and 4 in Figs. **A2** and **A3**); (3) Corsica and Sardina rotated some 30-33° counterclockwise with respect to Europe since the onset of Ligurian-Provençal rifting in Oligocene time (Dewey et al. 1989, Sérrane 1999, Schettino and Turco 2006 and many references therein). The pole of this rotation is located at or near the southern end of the Western Alpine Arc (Fig. **A11**), which was unaffected by Ligurian-Provençal rifting.

Previous workers have proposed the existence of a sinistral transform fault (Laubscher 1988, 1991) or a “sinistral extensional transfer domain” (Vignaroli et al. 2008) that accommodated opposing subductions beneath the Western Alps and

northern Apennines in Oligo-Miocene time. We differ with the view of Vignaroli et al (2008) that post-Eocene convergence in the Western Alps involved roll-back subduction, because there is no evidence in the foreland of the SW Alps for post-Eocene flexural response to an externally migrating foredeep (see comments of Molli et al. 2010, p. 29). Rather, we believe that post-Eocene shortening and arcuation of the Western Alps resulted primarily from collision and late Oligocene-Miocene indentation of the Adriatic Plate. Indentation was accommodated by coeval dextral Insubric deformation in the Central Alps (step 6, section 4.1.3) and sinistral displacement in the Ligurian Alps (section A4.3 below). Our reconstruction in Figure **10** adopts the basic idea of a transfer structure in the form of the sinistral Alps-Apennines Transfer (AAT in Figs. **10** and **A11**) as a kinematic necessity for accommodating post-late Oligocene rotations and broadly coeval, but opposite subduction directions on either side of the Alps-Apennines join.

Starting with this premise, we backrotate the Corsica-Sardinia block to its pre-late Oligocene position along the present European coast (Dewey et al. 1989), then connect the main faults on the "Alpine" part of Corsica (the Penninic and Piemont-Liguria Fronts) along nearly straight lines with equivalent fault segments in the Western Alps (Fig. **A10**) that underwent little, if any, rotation (segments b and c of Faults 3 and 4, Fig. **A2,** Aubourg and Chabert-Pelline 1999, Collombet et al. 2002). Segments of these faults that deviate from the straight-line geometry underwent counterclockwise rotation with respect to the AAT, whose trace was situated close to the Neogene rotation pole of the Corsica-Sardinia Block in Fig. **A11**. The orientation of the AAT is otherwise unconstrained, but we suspect that it trended no more easterly than the present-day Ligurian segment of the Western Alps (Fig. **A10**).

The CCW rotations of fault segments predicted in our reconstruction of the late Eocene Western Alps (56°, 80° and 120° in Fig. **A11**) compare reasonably well with the paleomagnetically determined post-30 Ma rotations for the same segments (respectively, 47°, 68° and 117° in Collombet et al. 2002). This is consistent with the notion that arcuation of the southwesternmost (Ligurian) part of the Western Alps resulted from a combination of northwestward Adriatic indentation of the Western Alps and southeastward retreat of the Apenninic subduction front in Oligo-Miocene time (Laubscher 2004). Apenninic roll-back subduction was probably responsible for a large amount of the extreme counterclockwise rotations of > 90° observed in the Ligurian Alps (section 4.3).

A4.3 Apenninic roll-back subduction and the Alps-Apennines Transfer Fault (AAT)

The Alps-Apennines junction has been called the "Ligurian knot" owing to its complex, three-dimensional structure (Laubscher et al. 1992). We define the Alps-Apennines Transfer fault (AAT) as the main structure that accommodated broadly coeval NW-directed Adriatic indentation of the Western Alps and SE-directed roll-back subduction in the northern Apennines (Fig. **10** and previous section)**.** Today, only a few deformed and rotated segments of this sinistral transfer fault are preserved in the Ligurian region (Fig. **2**) where they separate Penninic basement and ophiolitic units of the Ligurian Alps from "Liguride" units of the northern Apennines that override a Miocene accretionary prism (Molli et al. 2010, faults marked 2 in their fig. 7). These sinistral strike-slip fault segments were active in Oligocene to early- to mid-Miocene time according to stratigraphic criteria reviewed in Molli et al. (2010, their fig. 4). Motion on these faults coincided first with WNW- to NW-directed thrusting along the Penninic Front in the Western Alps (PN in Figs. **2** and **10**; Roselend Thrust of Ceriani et

al. 2001), and overlapped in time with rifting (24-20 Ma) and upper-plate spreading (20-16 Ma) of the Liguro-Provençal Basin (e.g., Séranne 1999) behind the eastwardly retreating Apenninic foredeep. This foredeep contained Chattian to lower Messinian clastic sediments (Molli et al. 2010) below the Apenninic thrust front, referred to by Schumacher and Laubscher (1996) as the "paleo-Apenninic" phase of thrusting and folding.

Although older ages have been proposed for the onset of Apenninic subduction (e.g., Late Cretaceous, Jolivet and Facenna 2000, Vignaroli et al. 2008; early Eocene, Lustrino et al. 2009), we follow most workers in favouring an early Oligocene age for this onset in the northern Apennines (e.g., Le Pichon et al. 1988, Gueguen et al. 1998, Michard et al. 2006, Schettino and Turco 2006, Molli 2008, Handy et al. 2010) based on the observation that east-vergent folds and thrusts in the northern Apennines overprint "Alpine" vergent structures of presumed late Eocene age (Elter and Pertusati 1973). An Eocene nappe complex with west-vergent Alpine thrusts is also well known on the eastern "Alpine" half of Corsica (e.g., Molli 2008) which experienced Neogene clockwise rotation away from a pre-Aquitanien orientation that was originally in line with the present European coastline (Sérrane 1999, Schettino and Turco 2006, Turco et al. 2012) as shown in Figures **8** of the main text and Fig. **A11**. The Cenozoic nappe structures in the Apennines were also laterally continuous with the internal core units of the Western and Central Alps (Fig. **8**) before being dissected by Apenninic thrusts and extensional faults during roll-back subduction (Fig. **10**). The predominance of Oligocene and younger calc-alkaline magmatic rocks in the Apennines (Lustrino et al. 2009, their fig. 3) supports the idea that the switch from Alpine to Apenninic subduction polarity occurred no earlier than 32 Ma (Molli 2008). Apenninic roll-back subduction was certainly active no later than 20-16 Ma, the age range of upper-plate spreading as noted above, probably already in Chattian time (28.5-23 Ma), and lasted until the Pliocene (Molli et al. 2010). The AAT is the likeliest candidate to have accommodated this roll-back subduction which induced Miocene counterclockwise rotation of the Corsica-Sardinia block.

As an aside, we note that an isolated occurrence of mid-Eocene subvolcanic rock in NW Sardinia (microdiorite at Calabona, 38.3 Ma Ar/Ar white-mica age of Lustrino et al. 2009) has been used by these and other authors to advocate that NW-directed Apeninnic subduction started in early Eocene time, while the SE-directed Alpine subduction on Corsica was still ongoing. Their scenario calls for an Eocene transform fault between Corsica and Sardina to accommodate the opposite subduction polarities. Although we cannot rule out this scenario, we consider it likelier that the Eocene Alpine subduction exposed on Corsica passes southward along strike to the east of Sardinia (Fig. **2**), which at that time was located in the lower plate of this SE-directed subduction (Fig. **8**). As mentioned in the previous section, rifting and subsidence in the upper plate of the Apenninic roll-back subduction did not start before early Oligocene time (34-32 Ma, e.g., Bois et al. 1993) and this agrees with the aforementioned predominance of Oligocene and younger rift-related magmatic rocks on Sardinia. The mid-Eocene subvolcanite at Calabona is therefore interpreted to manifest partial melting of the European slab, which may have delaminated and steepened to a position directly beneath Sardinia.

A combination of westward Adriatic indentation and eastward Apenninic roll-back subduction is proposed to have induced a sinistral shear couple at the Alps-Apennines join, effecting post-30 Ma counter-clockwise block rotations in the external, southwestern part of the Western Alpine arc (Ford et al. 2006) of more than 90-100° (Fig. **8**, e.g., Collombet et al. 2002), as summarized in the previous section. These rotations substantially accentuated the arc, which had started to form already in late

Eocene time at the northwestern corner of the advancing Alpine subduction front (Fig. **8**), where the subduction foredeep curved into a sinistral strike-slip shear zone bounding the western side of the orogen (Ricou and Siddans 1986, see also Ford et al. (2006, their fig. 5; and Handy et al. 2010, their fig. 14a). This initial bend increased during Adriatic indentation in latest Eocene-Oligocene to early Miocene time, when cold, exhumed upper mantle rocks of the Ivrea Zone ploughed into the already partly exhumed Alpine nappe stack of the Western Alps (Schmid and Kissling 2000, Ford et al. 2006). The ESE-dipping lithospheric slab beneath the Western Alps (Fig. **2**) continued to lengthen during northwestward motion of the Adriatic plate until the late Miocene. At that time, east-west shortening gave way to crustal extension in the Western Alps (Sue and Tricart 2003), possibly due to a third rupturing of the Alpine slab as manifested by the presently imaged discontinuity in the $+V_p$ anomaly beneath the Western Alps (Fig. **12e**, Lippitsch et al., 2003; Kissling et al., 2006). Pliocene-to-Quaternary thrusting in the northern Apennines (e.g., the Padinide thrust, Piana et al. 2000) has deformed and fragmented all older structures, including faults related to the AAT (e.g., Schumacher and Laubscher 1996).

A4.4 Restoring the Carpathians and Dinarides at 35 Ma, Alps-Dinarides Transfer Faulting (ADT2)

In the absence of Paleogene shortening constraints for the Carpathians and Dinarides, the main faults in Figure **8** were drawn according to the following procedure. In the Carpathians, the Mid-Hungarian Fault Zone was restored in two steps: (1) removal of 260 km of post-20 Ma dextral displacement according to the reconstruction of Ustaszewski et al. (2008) which used the Bükk Mountains and Medvednica Mountains units as markers that were originally contiguous and are presently situated on either side of the Mid-Hungarian Fault Zone (see composite Drina-Ivanjica-Bükk unit in the map legend of Schmid et al. 2008). The Miocene displacement of 260 km on the Mid-Hungarian Fault Zone is the difference between the 422 km presently separating these units (their fig. 2) and 162 km separating these markers in their reconstruction for 20 Ma (their fig. 6). Both units contain early Miocene volcanics (Seghedi et al. 2004, Kovac et al. 2007, their table 1) which provide convenient markers in Figures **8** and **10**; (2) restoration of much of the remaining (pre-20 Ma) distance between the Bükk and Medvednica Mountains units on either side of the Mid-Hungarian Fault Zone by bringing these into the closest possible proximity. This late Paleogene-early Neogene displacement is consistent with indications that the Mid-Hungarian Fault Zone accommodated Early Miocene dextral motion already before 20 Ma (Fodor et al. 1998), although other studies suggest that it was a south-directed thrust at this time (Csontos and Nagymarosy 1998). The combined effect of these two steps is to bring the Bükk and Medvednica Mountains with their early Miocene volcanics into approximate north-south alignment at about the same longitude as the Moesian Promontory and nearly coincident with the eastern boundary of the backrotated trace of the horizontalized Eastern Alpine slab (Fig. **8**, see also Fig. **A5**).

The second Alps-Dinarides Transfer Fault at 35 Ma (ADT2 in Fig. **8**) skirts the eastern edge of this horizontalized slab. The distances of the ADT2 and its predecessor, the ADT1 (see below, section A6.3), from the Moesian Promontory of the European Plate were fixed at the longitude of this promontory throughout the 35, 67 and 84 Ma time frames (Figs. **5, 6, 8**) because there is no evidence of significant pre-Neogene E-W

extension in the units between these faults and the promontory. During this time these units experienced dextral transpression.

The ADT2 linked the Alpine subduction of the Carpathian Embayment of Alpine Tethys belonging to the European Plate with the Dinaric collision and subduction of Adriatic continental lithosphere (Fig. **8**), i.e., it transferred north-directed thrusting of Austroalpine units on the Piemont-Valais-Magura units (exposed in the Pienides of northern Romania, Schmid et al. 2008, their fig. 1 and plate 1) to coeval southwest-vergent thrusting and folding in the Dinarides (e.g., Tomljenović et al. 2008). The Dinaric thrust front was located in the External Dinarides as documented by late Eocene-early Oligocene flysch presently found in offshore Montenegro and Albania (e.g., Picha 2002, Tari 2002, Carminati et al. 2004). However, late Paleogene thrusting also affected the Internal Dinarides as seen, for example, near the Moslavacka Gora Inselberg in Croatia, where the Tisza Unit is thrust onto Paleogene flysch of the Sava suture zone (Tomljenović et al. 2008, see also p. 161 of Schmid et al. 2008, their fig. 1 and plate 1). The northern part of the ADT2 is overprinted by the Mid-Hungarian Fault Zone which, as shown on Figures **2** and **10**, offsets the Adria-derived Medvenica and Bükk Mountain units (see Schmid et al. 2008, their plate 1).

In the Dinarides at 35 Ma, the West Vardar Obduction Front (WV) separated the Internal Dinarides in its hangingwall (comprising a stack of Middle Jurassic ophiolite-bearing nappes derived from the obducted remains of the West Vardar arm of Neotethys and imbricated with distal units of the Adriatic margin of Neotethys; East Bosnian-Durmitor and Drinja-Injanica/Korab-Pelagonian units of Schmid et al. 2008) from the External Dinarides in its footwall (comprising the Budva-Krasta-Cukali-Pindos Zone, the Dalmatian-Kruja-Gravrovo-Tripolitza Zone and the Ionian Zone).

Paleogene SW-directed thrusting in the Dinarides first affected the Internal Dinarides, as seen, for example, in the Kozara Inselberg in northern Bosnia and Hercegovina where Late Cretaceous ophiolites of the Sava suture Zone were thrust onto Thanetian to Lutetian turbiditic sandstones overlying the Western Vardar ophiolites (Ustaszewski et al. 2009, their figs. 3, 4 and 5; see also p. 161 of Schmid et al. 2008, their fig. 1 and plate 1). More external thrusts such as those at the base of the East-Bosnian/Durmitor and the more external Pre-Karst Unit were active from about Late Eocene to Early Oligocene time. This is documented by Late Eocene to Early Oligocene apatite fission track cooling ages from Thanetian to Lutetian flysch (see above) on top of the Western Vardar ophiolites (Ustaszewski et al. 2010, their figs. 5, 15 and table 1). By the late Eocene-early Oligocene, the Dinaric foredeep was located near the present-day Adriatic coast as indicated by flysch deposits presently found in offshore Montenegro and Albania (e.g., Picha 2002, Tari 2002, Carminati et al. 2004). This places the deformation front substantially more inland than at present. Based on the arguments above, we position the deformation front of the External Dinarides in the footwall of the West Vardar Obduction Front (WV), as shown in Figure **8**. However, we emphasize that there are substantial uncertainties regarding its exact location because no reliable shortening estimates are available.

Late Paleogene shortening in the External Dinarides (Fig. **8**) is estimated to be at least 90 km in the vicinity of Dubrovnik as obtained by subtracting 210 km of post-20 Ma shortening (Ustaszewski et al. (2008) from 300 km of post-late Eocene shortening at the same locality (minimum estimate of Schefer et al. 2011, p. 1200 based on profile 5 of plate 3 of Schmid et al. 2008). These crude shortening estimates in the Dinarides are very sensitive to the amount of Adria counterclockwise rotation assumed (20° in this study and Ustaszewski et al. 2008). Significantly less shortening across the Dinarides would be predicted for smaller angles of post-20 Ma counterclockwise rotation. Indeed,

recent plate motion studies suggest that this rotation was less than 20°, probably only about 10° (Eline Le Breton, personal communication). If so, the amount of post-20 Ma shortening reduces to only 100 km at the latitude of Dubrovnik. The presumed absence of significant Neogene shortening in the Internal Dinarides allows us to restore the trace of the Sava Zone in Figure **8** by maintaining the same distance between it and the WV as in our reconstruction for 20 Ma.

A4.5 Summary of Adriatic Plate motion for 35 Ma

Restoring Paleogene shortening in the Alps in step 6 yields a vector of 200 km to the NW (303°) for motion of Adriatic Plate relative to Europe from 35 to 20 Ma. This vector can be broken down into a westward component of 175 km and a northward component of 108 km. If we regard the total 35 Ma to present motion of Adria, then vector addition yields a motion of 308 km to the NW (311°), which can be broken down into a westward displacement of 227 km and a northward displacement of 205 km. These values agree within error (50 km) with the total length of the European slab imaged, respectively, in the ECORPS-CROP section (180-300 km) and the NFP20E section (180 km, Lippitsch et al. 2003, profiles A and B in their fig. 13).

We note that the 205 km northward component of this post-35 Ma motion vector is much greater than the previously estimated value of only 63 km used in Handy et al. (2010, calculated from their table 1) and contributes to straightening the Adriatic motion path at 35 Ma compared to the path in Handy et al. (2010, their fig. 7). This discrepancy partly reflects the aforementioned compatibility problems associated with restoration of the Western Alps (section 2.1 in the text, section A3.7 above), as well as our use of the total 75-95 km shortening values of Kempf and Pfiffner (2004) in retrodeforming the Helvetic nappes for the entire duration of Helvetic deformation (37-22 Ma) rather than the more modest 33 km value that Handy et al. (2010) took from Schmid et al. (1996, their table 1) for the time interval of 32-19 Ma.

Paleogene (Dinaric) shortening in the eastern part of the Southern Alps (Doglioni and Bosellini 1987) is not accounted for in our reconstruction because we are unaware of any published pre-Miocene shortening values in this region. If such shortening exists and were taken into account, then this would result in greater southward restoration and/or additional CW backrotation of the Adriatic Plate with respect to Europe in Figure **8**. The pre-Miocene orientation of faults and the amount of Paleogene shortening in the Carpathians and Dinarides are virtually unconstrained due to the lack of information and the complicated Miocene tectonics. More Paleogene shortening is possible than shown in Figure **8**, for example, if one were to assume that the subducted Adriatic margin of Neotethys originally extended to the east rather than to the ESE as shown.

A5. Map reconstruction at 67 Ma (Fig. 6 in the main text)

A5.1 Restoring subduction of Alpine Tethys from 35 Ma to 67 Ma (step 10)

Following the steps outlined in Handy et al. (2010), we restore the subduction of Alpine Tethys in Figure **6** by adding Late Cretaceous to Paleogene shortening along the NFP20E section in the Central Alps (315 km, Schmid et al. 1996, their table 1) to shortening estimates for Latest Cretaceous subduction of the Sesia Zone (150 km, Handy et al. 2010). The Sesia Zone (Fig. **A1**) is a piece of distal Adriatic margin that was

subducted and subsequently exhumed in Late Cretaceous to Paleogene time (Babist et al. 2006). This amounts to a retrotransation of 465 km to the SE (150°) of the Adriatic Plate at the city of Ivrea (Figs. **6** and **A6**).

Although this vector was derived for the Central Alps, it is probably also valid for the Eastern Alps, where Schmid et al. (2013) argue that the Alpine Tethys had a similar north-south width of about 500 km (Schmid et al. 1996). This is not inconsistent with an absolute minimum estimate of 205 km of Late-Cretaceous-Paleogene north-south shortening across the Eastern Alps, obtained by adding the subduction depths for Penninic oceanic and continental units in the Tauern Window (about 65 km each for the Glockner Nappe and Eclogite Zone at 42-45 Ma, Dachs and Proyer 2001, Hoschek 2001, Kurz et al. 2008) and the minimum amount (75 km) of thrusting of Austroalpine units onto the accreted Penninic units sometime between 50 and 35 Ma (Milnes 1978, Froitzheim et al. 1994).

The ADT1 is depicted in Figure **6** to have been aligned subparallel to the motion vector of Adria with respect to Europe at 67 Ma. The shape of the Austroalpine orogenic wedge north of the proto-Periadriatic Fault in this figure is practically unconstrained and is drawn to reflect the NNW- to NW-directed thrusting of the Austroalpine units onto the Penninic units, parallel to the NW-SE convergence direction of Adria and Europe (Handy et al. 2010, their fig. 5 and references cited therein).

A5.2 The European continental margins of Alpine Tethys

In the Alps, the European passive continental margin prior to Cenozoic collision is depicted to have been oriented approximately parallel to the trace of the Periadriatic Fault in Eocene time. This trace is shown in Figure **6** as a white dashed line that was obtained by projecting the Periadriatic Fault in Figure **8** onto the European slab at the same time slice (35 Ma), then horizontalizing this projection together with the slab. This operation reflects the notion that the Periadriatic Fault was situated directly above a late Eocene tear in the European slab that nucleated along the boundary between subducted continental and the oceanic lithospheres (von Blanckenburg and Davies 1995). Rupturing of the slab along this inherited weak zone channeled the rise of upwelling asthenosphere to the base of the orogenic crust, where mantle-derived melts interacted with the crust to produce the Oligocene, calc-alkaline intrusive suite localized along the Periadriatic Fault (von Blanckenburg and Davies 1995, Rosenberg 2004). The occurrence of early Neogene calc-alkaline magmatism in the Bükk Mountains unit of the eastern Pannonian Basin (Kovacs et al. 2007, their table 1) combined with the restored position of this unit along the eastward continuation of the Periadriatic Fault at 35 Ma (Fig. **8**) suggests that rupturing of the European slab propagated eastward into subducted oceanic lithosphere, possibly as far east as the Alps-Dinarides Transfer Fault, ADT1 (dashed line in Fig. **6**).

In western part of the Alpine domain, the European margin is depicted to have been somewhat wider in order to account for the large amount of crustal thickening and Eocene nappe stacking in the Lepontine part of the Central Alps and in the Tauern Window (Figs. **2, 5, 6**). In contrast, the geometry and width of the European margin in the Carpathians is poorly constrained. The northern margin of the Carpathian Embayment of Alpine Tethys is inferred to trend NE-SW, parallel to its overall trend in previous paleogeographic reconstructions (e.g., Schmid et al. 2008, Stampfli and Hochard 2009, Handy et al. 2010). The southeastern continental margin of this embayment includes the Tisza and Dacia units presently situated within the Carpathian

orogenic arc. The basement of this margin contains several thrust fronts of Cretaceous age (Figs. **5, 6**; Tisza-Dacia Front, TD; Eastern Vardar Obduction Front, EV, and Ceahlau-Severin Front, CS, Schmid et al. 2008 and references therein) that are shown to swing from their presently observed, NW-SE strike in the northern Dinarides into an originally NNE-SSW trend adjacent and parallel to the southern European margin of the Carpathian Embayment (Figs. **5, 6**). An original trend subparallel to the continental margin in late Cretaceous time is consistent with the notion that these sutures and fronts were zones of weakness that governed the localization of subsequent rifting and spreading of the Carpathian Embayment in late Jurassic-early Cretaceous time.

A5.3 The Adriatic continental margin of Neotethys

The eastern continental margin of Adria in Figure **6** trends at a small angle to the Adria-Europe convergence vector between 67 and 35 Ma, in keeping with the idea that the Dinaric collision was highly oblique. Paleogene shortening perpendicular to the Dinaric thrust belt was thus substantially less than the amount of convergence in the direction of relative plate motion. The Sava Zone is assumed to have become a suture in latest Cretaceous time based on the occurrence there of deformed and metamorphosed Maastrichtian sediments (70.6-65.5 Ma) that cooled from peak-metamorphism at about 65 Ma (Ustaszewski et al. 2010 and refs. therein).

A6. Map reconstruction at 84 Ma (Fig. 5 in the main text)

A6.1 Restoring subduction of part of the Adriatic margin, Alpine Tethys and Neotethys from 67 Ma to 84 Ma (step 11)

The motion vector of the Adriatic Plate at Ivrea is 150 km to the SE (150°) as determined by Handy et al. (2010, their table 1) based on their restoration of subduction depths for the three largest basement nappes of the Sesia Zone (Babist et al. 2006). This shortening estimate at the NW corner of the Adriatic continental block (Handy et al. 2010) is consistent with a minimum of 99 km of north-south directed, Late Cretaceous shortening further to the east in the Alps, including at least 35 km of south-directed Orobic thrusting in the Bergamasc part of the Southern Alps (Schönborn 1992) and 54 km of Late Cretaceous (90–72 Ma) north-directed thrusting in the Northern Calcareous Alps (Eisbacher et al. 1990).

A6.2 The Adriatic continental margin of Neotethys

At 84 Ma (Fig. **5**), the Adriatic continental margin of Neotethys is depicted with schematic transform offsets oriented at high angles to the trend of the rifted margin. This indicates that Neotethys spread in a north-south direction, i.e., at high angles to later spreading direction of Alpine Tethys. This northern branch of Neotethys is part of the Late Cretaceous Sava Ocean, a narrow back-arc basin that is proposed to have opened northeast of the southwestward-advancing Dinaric Arc and orogen (Schmid et al. 2008). Thus, we depict this back-arc basin as dissecting the previously obducted ophiolites of the western Vardar part of Neotethys (Fig. **5**).

A6.3 The first Alps-Dinarides Transfer Fault (ADT1)

The ADT1 at 84 Ma (Fig. **5**) is arbitrarily depicted to have an orientation parallel to the Adria-Europe convergence vector and subparallel to the trend of the rifted Adriatic margin adjacent to Neotethys (see above). The small wedge-shaped basin remaining between the ADT1 and the Tisza and Dacia Units of the European margin is a convenient setting for deposition of the Szolnok Flysch from Late Cretaceous to early Eocene time (Haas 2001). This flysch presently makes up part of the NE-SW trending segment of the Sava Zone that skirts the northern margin of the Tisza-Dacia Mega-unit buried beneath the Pannonian Basin ("ophiolite-bearing Intrapannonian belt" of Channell et al. 1979, Schmid et al. 2008, their plate 1). It comprises ophiolitic relics of the Sava Back-Arc Ocean, magmatic and metamorphic rocks, as well as Late Cretaceous deep marine red marls (Szentgyörgyi, 1989) that grade laterally into conglomerates and deep marine clastics (Schmid et al. 2008). We follow Schmid et al. (2008) in correlating the Szolnok Flysch with similar units in the "Pienides" of northern Romania (Sandulescu et al. 1981a; Tischler 2005; Tischler et al. 2007) and in the "Pennine" units beneath the East Slovak Basin (Inacovce-Krichevo Unit; i.e. Soták et al. 1999). All of these formations cover the nappes of the Tisza–Dacia block (Szepesházy 1973, Szentgyörgyi 1989, cited in Csontos and Nagymarosy, 1998) as depicted in Figures **5** and **6**. These troughs are interpreted as flexural basins that opened on the eastern active margin of the Eo-Alpine orogenic wedge.

B. Reconstructing slab geometries beneath the Alps

B1. Procedure

To locate the lithospheric slabs beneath the Western and Eastern Alps prior to subduction, we first determine the present orientation of the slabs in tomographic images (step 1), then rotate them into a horizontal attitude (step 2). The location of the slabs before subduction is then obtained by translating and rotating their horizontalized images with respect to an appropriate crustal reference frame (Europe, stable Adria) in accordance with the amount, direction and timing of lithospheric shortening related to the subduction (step 3). This step is repeated for earlier deformational fields to obtain locations of the horizontalized Eastern Alps slab even further back in time (steps 4-7).

B2. Retrodeforming the slabs beneath the Alps

B.2.1 Defining slabs from tomographic sections (step 1)

The Western Alps and Eastern Alps slabs are imaged in the high-resolution teleseismic tomograms of Lippitsch et al. (2003) as shown in the horizontal depth slices in Figure **B1** and the cross sections in Figure **B2**. Figure **B3** depicts contours of the slabs projected to the surface (thin coloured lines). These contours correspond to the 4% V_p anomaly contours, i.e., the margin of the blue domains in the tomographic depth slices. The thick coloured lines represent the horizontalized edges of the Western Alps (blue)

and Eastern Alps (red) slabs. We use only the contours of the slabs' upper surfaces to obtain the slab dips, but note that full contours of the tops, bottoms and sides of the labs outline complex three-dimensional shapes, as discussed below.

B2.2 Horizontalizing the slabs (step 2)

To horizontalize the slabs, we must determine their edges, lengths and dips, preferably in the direction of subduction. This further requires that we locate the hinges or axes of slab rotation in the tomograms.

B2.2.1 Western Alps slab:

Figure **B1** and the published tomographic cross sections of Lippitsch et al. (2003) reveal that the European slab beneath the Western Alps is partly detached, but maintains its integrity as a single, SE-dipping slab beneath the Central Alps. In this study, we focus on the undetached part as discussed in the main text. In Figure **B2a**, the 2% $+V_p$ anomaly contour defines the bottom end of the undetached part of the European slab at a depth of about 210 km. We chose this contour, rather than the 5% contour, to represent the slab edge in profile because of the geometrical distortion and amplitude reduction of the slab image related to the large cell size (50 x 50 x 30 km) that only partly contains slab material. The length of the slab (160 km) is then measured between the slab edge (grey circle) and the slab hinge (red circle) in cross section. The slab hinge is located halfway along a thin black line representing the shortest distance between the base of the down-going slab and the junction of the European and Adriatic Mohos (intersection of red lines in Fig. **B2**). The Moho in all cross sections was drawn using an optimization procedure that combines controlled-source seismology and receiver function information (Spada et al. 2013). We note that the thin black lines constructed like this approximate the axial trace of the fold defined by unsubducted and subducted parts of the down-going lithosphere.

The axis used to rotate the European slab into a horizontal orientation trends N45°E, i.e., parallel to the average trace of the slab tip in the 210 km depth slice (Fig. **B1b**). The rotational angle corresponding to the slab dip is about 55° looking NE along the rotational axis. This axis is reasonable given that its trend is approximately perpendicular to the direction of Neogene subduction in the western part of the Central Alps (Schmid et al. 1996, Schmid and Kissling 2000, Handy et al. 2010).

After rotation, the horizontalized trace of the slab's edge in the 210 km tomographic slice comes to rest 160 km to the SE of the rotational axis, a distance equivalent to its present-day length (Fig. **B3**). Note that the length of the European slab in the direction of subduction yields an independent measure of shortening in the Central Alps since slab break-off in late Eocene time. The slab length parallel to the SE-ward direction of subduction was used in our map reconstructions as the distance between the edge of the European margin and the present Alpine thrust front at the base of the Subalpine Molasse.

B2.2.2 Eastern Alps slab:

Restoring the Eastern Alps slab to its pre-subduction orientation is notoriously difficult due to its complex three-dimensional geometry. The tomographic depth slices and cross sections indicate that both the strike and dip of the slab vary in map view. The shape of the slab also changes with depth, from elongate at 150 km, to tabular at 210 km, to almost circular at 240 km depth (Schmid et al. 2008, their plate 1; Fig. **B1**). Thus, the strike of this slab can only be defined where it is elongate to tabular in map view, i.e., at depths of 150 to 210 km. The depth of the slab's leading edge decreases going from east (240-250 km, Fig. **B2c**) to west (210 km at 12.5°E, Fig. **B2d**). The depth contours converge towards the western and eastern ends of the slab, indicating that it dips subvertically at both ends. In the TRANSALP section at 11.5°E, the high V_p anomaly dips subvertically (Fig. **B2b**), and receiver functions (Kummerow et al. 2004) and local earthquake tomography (Diehl et al. 2009) indicate that the through-going Moho dips to the south, in accordance with S- to SE-directed subduction of the European lithosphere. The subvertical slab anomaly in this section is weaker and shorter than in other sections (Fig. **B2b**), and indeed, may be interpreted either as of European or Adriatic origin.

Thus, a clearly imaged N-dipping slab beneath the Eastern Alps extends westward no further than about 12.5°E, but is imaged eastward to at least 16°E, where tomographic resolution becomes poor (Fig. **B1**). In view of this complexity, our attempt below to define a single rotation axis for the purpose of horizontalizing the slab must be regarded as an unavoidable simplification pending a better characterization of the slab geometry.

We use the elongate direction of the slab contours at 210 km together with the criteria above for the hinge of the slab to define the N280°W trend of the horizontal rotational axis at 80 km depth (Figs. **B2c, d** and **B3**). This axis trends parallel to the surface trace of the Periadriatic Fault as well as to an elongate zone of low crustal velocity gradient that preclude the definition of a Moho beneath part of the Eastern Alps (Spada et al. 2013). We attach no geological significance to the coincidence of these features other than to note that both strike-slip motion along the Periadriatic Fault and subduction of the Eastern Alps slab occurred during Neogene time (see discussion in text).

To horizontalize the slab, we rotated three points situated along the present-day edge of the slab and at right angles to the rotational axis (grey circles on thin red lines in Figs. **B2c** and **B3**): one point at 210 km near the western end of the slab and two others located at 240 km along the northern and eastern segments of its edge. The dip and length of the slab in the three sections containing these points were then calculated simply from knowledge of the depth of the rotation axis (80 km), the depth of the points along the slab edge (above) and the horizontal distance separating the axis from the surface projections of the points. As expected, the dip and length of the slab vary along the rotation axis (Fig. **B3**). Obviously, these values are not the same as those measured in existing tomographic cross sections in Figure **B2** because the latter are not oriented perpendicular to the rotational axis. The amount of rotation (clockwise looking ESE) needed to horizontalize the three points along the slab edge varies from 58° in the west, to 53° in the middle, to 73° near the eastern limit of the slab. A consequence of this differential rotation about a common horizontal rotation axis is that the slab underwent shearing during oblique subduction and indentation, as discussed in the text.

To obtain a continuous outline of the horizontalized slab edge, we interpolate between the rotated points (open circles along thick red line in Fig. **B3**). The result is an arcuate leading edge that comes to rest some 150 to 200 km north of the rotational axis and just beyond the present Alpine Front in the Eastern Alps (**Fig. 10** in text).

B2.3 Restoring the horizontalized slab to position at 20 Ma (step 3)

To restore the horizontalized Eastern Alps slab to its location before subduction beneath the Eastern Alps, we retrotranslate it 113 km to the S55°E (vector determined in part 1 of the Appendix), then backrotate it by 20° CW about a vertical axis at the city of Ivrea (Fig. **B4**). This translation and rotation are taken from the estimates of differential Neogene shortening in the Southern Alps and Dinarides, as discussed in the text and part 1 of the Appendix (Note: steps outlined here for slab restoration are numbered differently than the steps for plate motion reconstruction). Implicit in this operation is the assumption that the slab beneath the Eastern Alps was attached to the stable part of the Adriatic microplate and therefore moved with respect to Europe. The Cenozoic-to-Recent European plate is defined as all units north of the Periadriatic Fault, including units of former Adriatic affinity that were accreted to the Alpine orogenic wedge in pre-Neogene time. The restored tip of the horizontalized slab thus comes to rest at the northeast corner of the Adriatic microplate, just north of the Periadriatic Fault.

B2.4 Restoring the horizontalized slab to positions at 35, 67 and 84 Ma (steps 4-6)

Restoring the horizontalized Eastern Alps slab back to its locations at 35 Ma, 67 Ma and 84 Ma (Figs. **5**, **6** and **10** in the main text) is achieved by subjecting it to the same retrotranslations as the Adriatic microplate during this time interval. These are described in the text and in section A above. In other words, the slab is fixed to the Adriatic microplate and moves with it with respect to Europe. These retrotranslations are shown in Figures **B5** (35 Ma), **B6** (67 Ma) and **B7** (84 Ma).

C. Other models for the origin of the slab anomaly beneath the Eastern Alps

Recent interpretations that invoke "classical" south- to southeast-directed subduction of European lithosphere to explain the subcrustal structure of the Eastern Alps are based on different interpretations of Moho images (Brückl et al. 2010) and mantle tomography (Mitterbauer et al. 2011) in the Eastern Alps-Pannonian area. The latter authors employed an expanded seismometer network augmented by temporary stations east of 14°E and in the Pannonian area (ALPASS teleseismic experiment). Based on their preferred model (ALPASS model in their fig. 9), they concluded that the $+V_p$ anomaly beneath the Eastern Alps extends down to 250 km and changes dip continuously along strike from steeply south-dipping (80°) in the west (9°E) to subvertical or steeply north- dipping in the east (12-14°E). Like Lippitsch et al. (2003) before, Mitterbauer et al. (2011) imaged lower positive velocities between the slabs in the Central and Eastern Alps, but they question whether this gap signifies two separate slabs. Rather, they argue that the slab beneath the Eastern Alps is the lateral equivalent of the European slab beneath the Central Alps because its length of 200 km closely matches the 190 km of Neogene north-south crustal shortening in the Eastern Alps proposed by Ustaszewski et al. (2008). They note that the Eastern Alpine slab anomaly follows the offset of the European and Adriatic Mohos, which as imaged by Brückl et al. (2010) indicates uniformly S-directed European subduction.

We are not convinced by this line of argumentation for the following reasons:

(1) Decreased intensity of $+V_p$ anomalies between the Central and Eastern Alps is a robust feature of all models and separates two distinct slab anomalies, as indicated by the contoured $+V_p$ anomaly values in the model of Lippitsch et al. (2003) which are 2-3 times greater than in the preferred ALPASS model of Mitterbauer et al. (2011, compare V_p contour values in their fig. 9);
(2) In the Eastern Alps, a Moho offset indicating subduction of European lithosphere beneath the Adriatic Plate is only imaged south of the western Tauern Window (Lüschen et al. 2004, Kummerow et al. 2004), but not between about 12°E and 15°E where no Moho discontinuity can be imaged unambiguously (Spada et al. 2013). As discussed in section 5 of this paper, the missing Moho in this area may be diagnostic of lower crust that was detached and imbricated during the Miocene change in subduction polarity beneath the Eastern Alps;
(3) If a continuous, south-dipping European slab beneath the Eastern Alps ever existed in Miocene time, then the remaining part of this slab must have rotated into its current subvertical to north-dipping attitude since then. The mechanisms of such rotation and verticalization are unclear; either the slab was twisted and pulled down by a still deeper slab anomaly below 350 km depth beneath the Pannonian basin (Mitterbauer et al. 2011) or it rotated on its end when it was overridden by the European lithosphere. The former explanation is inconsistent with the evidence for two originally independent slabs (above), whereas the latter would necessitate southward motion of Europe with respect both to the slab and to the Adriatic Plate. Such motion does not fit with plate motion studies indicating that during the Neogene both Eurasia and Adria moved to the northeast in an absolute Atlantic/India hotspot reference frame (Torsvik et al. 2008, their table 4). This northeastward motion precludes overturning of a Miocene south-dipping European slab beneath the Eastern Alps and in fact would be expected to exert a southwest-directed asthenospheric drag force on the slab, leading to a shallower rather than steeper dip of a hypothetically south-dipping slab beneath the Eastern Alps;
(4) The near coincidence in the length of the slab anomaly and the amount of post-20 Ma shortening in the Eastern Alps (Mitterbauer et al. 2011) is only a valid criterion for ascertaining the European or Adriatic affinity of the slab if the subduction polarity is known and the locus of shortening in the Alps is specified. Ustaszewski et al. (2008) point out that about 190 km of Neogene shortening was accommodated in the Southern Alps and the Tauern Window above a north-dipping slab anomaly, which is consistent with an Adriatic provenance of this anomaly.

Another potential objection to north-directed subduction of Adriatic lithosphere beneath the Eastern Alps is the lack of a large foredeep with Molasse-type sedimentation in the eastern part of the Southern Alps. Such a foredeep would be expected to develop as a flexural response to the mass of the downgoing slab beneath the Eastern Alps. In fact, a Neogene-Quaternary basin exists in the Adriatic-Friuli foreland (Merlini et al. 2002), but its maximum depth (1.2 km in their fig. 2) and areal extent are admittedly modest if one assumes that the entire approximately 200-240 km length of slab beneath the Eastern Alps is all derived from Adriatic lithosphere.

Modelling the flexural response to slab loading in this complex area at the Alps-Dinarides junction is an interesting challenge, especially because any model will have to account for the fact that the lithosphere is transected by several Miocene and older

strike-slip and oblique-slip faults (e.g., the Periadriatic Fault, PF in Fig. **10**). In the Eastern and Southern Alps, these faults continue to accommodate north-south shortening associated with Adria-Europe convergence by allowing orogen-parallel extrusion of the Eastern Alps towards the Pannonian basin (e.g., Fodor et al. 1998, Vrabec et al. 2006, Caporali et al. 2013). The dextral strike-slip faults in the northern Dinarides also take up part of the northward motion of the Adriatic Plate (Grenerzcy et al. 2005, Kastelic et al. 2008). All of these structures are expected to weaken the coupling of the Southern Alps foreland with the slab beneath the Eastern Alps, effectively decreasing the rigidity of the lithosphere and severely damping the flexural response of the foreland to slab loading. Under these circumstances, it seems hardly surprising that no large Miocene foreland basin has developed in the eastern part of the Southern Alps.

Alternatively, the modest flexural response of the Southern Alps foreland may reflect a smaller amount of subduction than the 200-240 km length of slab in the tomographic maps and sections in Figures **B1** and **B2d** would suggest. If so, then the observed flexural response of the Southern Alps foreland may even allow a rough calculation of the amount of north-directed subduction (B. Fügenschuh, personal communication).

To summarize, several lines of reasoning cast doubt on the classical concept of continuous subduction of European lithosphere beneath the Eastern Alps. The available evidence supports the interpretation of an early Miocene reversal in subduction polarity, with Adriatic continental lithosphere subducting to the north since 20-23 Ma.

D. References

Anderson H, Jackson L (1987) Active tectonics of the Adriatic region, Geophys J R Astron Soc 91: 937– 983

Argand E (1916) Sur l'arc des Alpes Occidentales. Eclogae Geol Helv 14: 145

Aubourg C, Chabert-Pelline C (1999) Neogene remagnetization of normal polarity in the Late Jurassic black shales from the Subalpine chains (French Alps): evidence for late anticlockwise rotations. Tectonophysics 308: 473–486

Babić L, Hernitz-Kučenjak M, Ćorić S, Zupanič J (2007) The Middle Eocene Age of the Supposed Late Oligocene Sediments in the Flysch of the Pazin Basin (Istria, Outer Dinarides). Natura Croatica 16 (2): 83-103

Babist J, Handy MR, Konrad-Schmolke M, Hammerschmidt K (2006) Precollisional multistage exhumation of the subducted continental crust: the Sesia zone, western Alps. Tectonics 26: TC6008. doi:10.1029/2005TC001927

Becker A (2000) The Jura Mountains - an active foreland fold-and-thrust belt? Tectonophysics 321: 381-406

Bois C (1993) Initiation and evolution of the Oligo-Miocene rift basins of southwestern Europe: Contribution of deep seismic reflection profiling. Tectonophysics 226: 227 – 252

Broadley L, Platzman ES, Platt JP, Papanikolaou M, Matthews S (2006) Paleomagnetism and the tectonic evolution of the Ionian zone, northwestern Greece. Geol Soc Am Special Paper 409: 137–155, doi:10.1130/2006.2409(08)

Brückl E, Behm M, Decker K, Grad M, Guterch A, Keller GR, Thybo H (2010) Crustal structure and active tectonics in the Eastern Alps. Tectonics 29: TC2011. doi:10.1029/2009TC002491

Burchfiel BC, Nakov R, Durmurdzanov N, Papanikolaou D, Tzankov T, Serafimovski T, King RW, Kotzev V, Todosov A, Nurce B (2008) Evolution and dynamics of the Cenozoic tectonics of the Southern Balkan extensional system. Geosphere 4(6): 919-938

Burkhard M (1990) Aspects of the large-scale Miocene deformation in the most external part of the Swiss Alps (Subalpine Molasse to Jura fold belt). Eclogae Geol Helv 83: 559–583

Burkhard M, Sommaruga A (1998) Evolution of the western Swiss Molasse basin: structural relations with the Alps and the Jura belt. Geol. Soc Lond Sp Publ 134: 279–298

Calais E, Nocquet JM, Jouanne F, Tardy M (2002) Current strain regime in the Western Alps from continuous Global Positioning System measurements, 1996-2001. Geology 30(7): 651-654

Caporali A, Neubauer F, Ostini L, Stangl G, Zuliani D (2013) Modeling surface GPS velocities in the Southern and Eastern Alps by finite dislocations at crustal depths. Tectonophysics 590: 136-150

Castellarin A, Vai GB, Cantelli L (2006) The Alpine evolution of the Southern Alps around the Giudicarie faults: A Late Cretaceous to Early Eocene transfer zone. Tectonophysics 414 (1-4): 203-223

Channel JET, D'Argenio B, Horváth F (1979) Adria, the African promontory, in Mesozoic Mediterranean paleogeography. Earth Science Reviews 15(3): 213-292

Ceriani S, Fügenschuh B, Schmid SM (2001) Multi-stage thrusting at the "Penninic Front" in the Western Alps between Mont Blanc and Pelvoux massifs. Int J Earth Sci 90: 685–702

Ceriani S, Schmid SM (2004) From N-S collision to WNW-directed post-collisional thrusting and folding: Structural study of the Frontal Penninic Units in Savoie (Western Alps, France). Eclogae Geol Helv 97: 347–369

Chorowicz J (1970) La transversale de Zrmanja (Yougoslavie). Bulletin de la Société Géologique de France 12(6): 1028–1033

Chorowicz J (1975) Mechanics of Split-Karlovac transversal structure in Yugoslavian Dinarides. Compte-Rendu Académie des Sciences, Série D 280(20): 2313–2316

Collombet M, Thomas JC, Chauvin A, Tricart P, Bouillin JP, Gratier JP (2002) Counterclockwise rotation of the western Alps since the Oligocene: New insights from paleomagnetic data. Tectonics 21(4): 10.1029/2001TC901016

Csontos L, Nagymarosy A (1998) The Mid-Hungarian line: a zone of repeated tectonic inversions. Tectonophysics 297: 51-71

Dachs E, Proyer A (2001) Relics of high-pressure metamorphism from the Grossglockner region, Hohe Tauern, Austria: Paragenetic evolution and PT-paths of retrogressed eclogites. European Journal of Mineralogy 13: 67–86

de Leeuw A, Mandić O, Krijgsman W, Kuiper K, Hrvatović H (2012) Paleomagnetic and geochronologic constraints on the geodynamic evolution of the Central Dinarides. Tectonophysics 530–531: 286-298

Dewey JF, Helman ML, Turco E, Hutton DHW, Knott SD (1989) Kinematics of the Western Mediterranean. Geol Soc Lond Sp Publ 45: 265–283

Diehl T, Kissling E, Husen S, Aldersons F (2009) Consistent phase picking for regional tomography models: application to the greater Alpine region, Geophys J Int 176: 542-554

Doglioni C, Bosellini A (1987) Eoalpine and mesoalpine tectonics in the Southern Alps. Geol Rundschau 76(3): 735-754

Eisbacher GH, Linzer HG, Meier L, Polinski R, (1990) A depth-extrapolated structural transect across the Northern Calcareous Alps of western Tyrol. Eclogae Geol Helv 83 (3): 711–725

Elter P, Pertusati PC (1973) Considerazioni sul limite Alpi-Appennino e sulle sue relazioni con l'arco delle Alpi Occidentali. Memorie della Società Geologica Italiana 12: 359–375

Fodor L, Jelen B, Márton E, Skaberne D, Čar J, Vrabec M (1998) Miocene-Pliocene tectonic evolution of the Slovenian Periadriatic fault: Implications for Alpine-Carpathian extrusion models. Tectonics 17(5): 690-709

Ford M, Duchêne S, Gasquet D, Vanderhaeghe O (2006) Two-phase orogenic convergence in the external and internal SW Alps. J Geol Soc Lond 163: 815-826

Frisch W, Kuhlemann J, Dunkl I, Brügel A (1998) Palinspastic reconstruction and topographic evolution of the Eastern Alps during late Tertiary tectonic extrusion. Tectonophysics 297: 1-15

Froitzheim N, Schmid SM, Frey M (1996) Mesozoic paleogeography and the timing of eclogite facies metamorphism in the Alps: A working hypothesis. Eclogae Geol Helv 89: 81-110

Fügenschuh B, Schmid SM (2005) Age and significance of core complex formation in a very curved orogen: Evidence from fission track studies in the South Carpathians (Romania). Tectonophysics 404: 33– 53

Fügenschuh B, Seward D Mancktelow SD (1997) Exhumation in a convergent orogen: The western Tauern Window. Terra Nova 9: 213 – 217, doi:10.1046/j.1365-3121.1997.d01-33.x

Gawlick HJ, Frisch W, Vecsei A, Steiger T, Böhm F (1999) The change from rifting to thrusting in the Northern Calcareous Alps as recorded in Jurassic sediments. Geol Rundschau 87: 644-657

Gouffon Y (1993) Géologie de la nappe du Grand Saint-Bernard entre le val de Bagnes et la frontier Suisse (Vallée d'Aoste, Italie). Mem Géol Lausanne 12: 1-147

Grasemann B, Mancktelow N (1993) Two-dimensional thermal modelling of normal faulting: The Simplon Fault Zone, central Alps, Switzerland. Tectonophysics 235: 155-165

Gratier JP, Ménard G, Arpin R (1989) Strain-Displacement Compatibility And Restoration Of The Chaines Subalpines Of The Western Alps. Geol Soc Lond Spec Publ 45: 65-81

Grenerczy, G., Sella, G., Stein, S., Kenyeres, A. (2005), Tectonic implications of the GPS velocity field in the northern Adriatic region. Geophys Res Lett *32*(L16311): doi:10.1029/2005GL022947

Gueguen E, Doglioni C, Fernandez M (1998) On the post-25 Ma geodynamic evolution of the western Mediterranean. Tectonophysics 298: 259-269

Haas J, Hamor G, Jambor A, Kovacs S, Nagymarosy A, Szenderkenyi T (2001) Geology of Hungary, Eötvös University Press, Budapest, 317pp.

Handy MR, Babist J, Wagner R, Rosenberg CL, Konrad-Schmolke M (2005) Decoupling and its relation to strain partitioning in continental lithosphere: insight from the Periadriatic fault system (European Alps). Geol Soc Lond Spec Publ 243: 249–276

Handy MR, Schmid SM, Bousquet R, Kissling E, Bernoulli D (2010) Reconciling plate-tectonic reconstructions with the geological-geophysical record of spreading and subduction in the Alps. Earth Sci Rev 102: 121-158

Hitz L, Pfiffner OA (1995) The 3D crustal structure of the Alps of eastern Switzerland and western Austria interpreted from a network of deep-seismic profiles. Tectonophysics 248: 71-96

Horváth F, Bada G, Szafián P, Tari G, Ádám A, Cloetingh S (2006) Formation and deformation of the Pannonian Basin: constraints from observational data. Geol Soc Lond Mem 32: 191-206

Hoschek G, (2001) Thermobarometry of metasediments and metabasites from the eclogite zone of the Hohe Tauern, Eastern Alps, Austria. Lithos 59: 127–150

Jouanne F, Mugnier JL, Koci R, Bushati S, Matev K, Kuka N, Shinko I, Kociu S, Duni L (2012) GPS constraints on current tectonics of Albania. Tectonophysics 554–557: 50-62

Kastelic V, Vrabec M, Cunningham D, Gosar A (2008) Neo-Alpine structural evolution and present-day tectonic activity of the eastern Southern Alps: The case of the Ravne Fault, NW Slovenia. J Struct Geol 30: 963-975

Kempf O, Pfiffner OA (2004) EarlyTertiary evolution of the North Alpine Foreland Basin of the Swiss Alps and adjoining areas. Basin Research 16: 549–567, doi: 10.1111/j.1365-2117.2004.00246.x

Kissel C, Laj C (1988) The Tertiary geodynamical evolution of the Aegean arc: A paleomagnetic reconstruction. Tectonophysics 146: 183–201, doi:10.1016/0040-1951(88)90090-X

Kissel C, Speranza F, Milicevic V (1995) Paleomagnetism of external southern and central Dinarides and northern Albanides: Implications for the Cenozoic activity of the Scutari-Peç transverse zone. J Geophys Res 100: 14999-15007

Kissling E, Schmid SM, Lippisch R, Ansorge J, Fügenschuh B (2006) Lithosphere structure and tectonic evolution of the Alpine arc: new evidence from high-resolution teleseismic tomography. Geol Soc Lond Mem 32: 129-145

Kovács I, Csontos L, Szabó C, Bali E, Falus G, Benedek K, Zajacz Z (2007) Paleogene-early Miocene igneous rocks and geodynamics of the Alpine-Carpathian-Pannonian-Dinaric region: An integrated approach. Geol Soc Am Special Paper pp 93-112

Kummerow J, Kind R, Oncken O, Giese P, Tyberg T, Wylegalla K, Scherbaum F,, TRANSALP Working Group (2004) A natural and controlled source seismic profile through the Eastern Alps: TRANSALP. Earth Planet Sci Lett 225: 115–129

Kurz W, Handler R, Bertoldi C (2008) Tracing the exhumation of the Eclogite Zone (Tauern Window, Eastern Alps) by 40Ar/39Ar dating of white mica in eclogites. Swiss J Geosci 101:191–206

Laubscher HP (1971) Das Alpen-Dinariden Problem und die Palinspastik der südlichen Tethys. Geol Rundschau 60: 813-833

Laubscher HP (1988) The arcs of the Western Alps and the North Apennines: an updated view. Tectonophysics 146(10): 67-78

Laubscher HP (1991) The arc of the Western Alps today. Eclogae Geol Helv 84(3): 631-659

Laubscher HP, Biella GC, Cassinis R, Gelati R, Lozej A, Scarascia S, Tabaco I (1992) The collisional knot in Liguria. Geol Rundschau 81(2): 275-289

Leloup PH, Arnaud N, Sobel ER, Lacassin R (2005) Alpine thermal and structural evolution of the highest external crystalline massif: The Mont Blanc. Tectonics 24: 4, DOI: 10.1029/2004TC001676

Le Pichon X, Bergerat F, Roulet MJ (1988) Plate kinematics and tectonics leading to the Alpine belt formation; A new analysis, in Processes in Continental Lithospheric Deformation. Geol Soc Am Special Paper 218: 111 – 131

Lickorish W, Ford M (1998) Sequential restoration of the external Alpine Digne thrust system, SE France, constrained by kinematic data and synorogenic sediments. Geol Soc Lond Spec Publ 134: 189–211

Linzer HG, Decker K, Peresson H, Dell'Mour R, Frisch W (2002) Balancing lateral orogenic float of the Eastern Alps. Tectonophysics 354: 211-237

Lippitsch R, Kissling E, Ansorge J (2003) Upper mantle structure beneath the Alpine orogen from high-resolution teleseismic tomography. J Geophys Res 108: doi: 10.1029/2002JB002016

Loprieno A, Bousquet R, Bucher S, Ceriani S, Dalla Torre FH, Fügenschuh B, Schmid SM (2011) The Valais units in Savoy (France): a key area for understanding the palaeogeography and the tectonic evolution of the Western Alps. Int J Earth Sci 100: 963–992

Luciani V, Silvestrini A (1996) Planktonic foraminiferal biostratigraphy and paleoclimatology of the Oligocene/Miocene transition from the Monte Brione Formation (northern Italy, Lake Garda). Mem Sci Geol 48: 155–169

Lustrino M, Morra V, Fedele L, Franciosi L (2009) Beginning of the Apennine subduction system in central western Mediterranean: Constraints from Cenozoic ‘‘orogenic’’ magmatic activity of Sardinia, Italy. Tectonics 28: TC5016, doi:10.1029/2008TC002419

Lüschen E, Lammerer B, Gebrande H, Millahn K, Nicolich R, TRANSALP Working Group 1 (2004) Orogenic structure of the Eastern Alps, Europe, from TRANSALP deep seismic reflection profiling. Tectonophysics 388 (1-4): 85-102

Madritsch H, Schmid SM Fabbri O (2008) Interactions between thin- and thick-skinned tectonics at the northwestern front of the Jura fold-and-thrust belt (eastern France). Tectonics 27: TC5005

Mandl G (2000) The Alpine Sector of the Tethyan shelf—Examples of Triassic to Jurassic sedimentation and deformation from the Northern Calcareous Alps. Mitt Österr Geo Ges 92: 61–77

Márton E, Zampieri D, Grandesso P, Ćosović V, Moro A (2010) New Cretaceous paleomagnetic results from the foreland of the Southern Alps and the refined apparent polar wander path for stable Adria. Tectonophysics 480: 57–72

Márton E, Zampieri D, Kázmér M, Dunkl I, Frisch W (2011) New Paleocene-Eocene paleomagnetic results from the foreland of the Southern Alps confirm decoupling of stable Adria from the African plate. Tectonophysics 504: 89-99

Merlini S, Doglioni C, Fantoni R, Ponton M (2002) Analisi strutturale lungo un profilo geologico tra la linea Fella-Sava e l'avampaese adriatico (Friuli Venezia Giulia-Italia). Mem Soc Geol Italia 57: 293-300

Michard A, Negro F, Saddiqi O, Bouybaouene ML, Chalouan A, Montigny R, Goffé B (2006) Pressure–temperature–time constraints on the Maghrebide mountain building: evidence from the Rif–Betic transect (Morocco, Spain), Algerian correlations, and geodynamic implications. C R Geoscience 338: 92-114

Mikes T, Dunkl I, von Eynatten H, Báldi-Beke M, Kázmer M (2008) Calcareous nannofossil age constraints on Miocene flysch sedimentation in the Outer Dinarides (Slovenia, Croatia, Bosnia-Hercegovina and Montenegro). Geol Soc Lond Spec Publ 298: 335–363

Milnes AG (1978) Structural zones and continental collison, Central Alps. Tectonophysics 47: 369-392

Mitterbauer U, Behm, M, Brückl E, Lippitsch R, Guterch A, Keller GR, Koslovskaya E, Rumpfhuber EM, Sumanovac F (2011) Shape and origin of the East-Alp slab constrained by the ALPASS teleseismic model. Tectonophysics 510: 195-206

Molli G (2008) Northern Apennine-Corsica orogenic system: an updated overview. Geol Soc Lond Spec Publ 298: 413-442

Molli G, Crispini L, Malusà MG, Mosca MG, Piana F, Federico L (2010) Geology of the Western Alps-Northern Apennine junction area – a regional review. Journal of the Virtual Explorer 36 (10): 1-49, doi:10.3809/jvirtex.2010.00215

Nussbaum C (2000) Neogene tectonics and thermal maturity of sediments of the easternmost Southern Alps (Friuli Area, Italy). PhD Thesis, Université de Neuchâtel, Neuchâtel, Switzerland, 172 pp

Piana F (2000) Structural setting of western Monferrato (Alps-Apennines junction zone, NW Italy). Tectonics 19: 943 – 960

Pieri M, Groppi G (1981) Subsurface geological structure of the Po Plain, Italy. Prog Final Geodin Publ 414: 1-13

Pfiffner OA (1986) Evolution of the north Alpine foreland basin in the Central Alps. Sp Publ Int Assoc Sedimentol 8: 219 – 228

Pfiffner OA (2009) Geologie der Alpen. Haupt Verlag, Bern, 359 pp

Philippe Y, Coletta B, Deville E, Mascle A (1996) The Jura fold-and-thrust belt: a kinematic model based on map-balancing. Ziegler PA, Horváth F (eds) Peri-Tethys Memoire 2. Mém Mus Natn Hist Nat Paris 170: 235–261.

Piromallo C, Morelli A (2003) P-wave tomography of the mantle under the Alpine Mediterranean area. J Geophys Res 108 (B2): doi:10.1029/2002JB001757

Polšak M, Jurisa M, Sparica M, Simunic A (1976) Sheet "Bihac", 1:100.000, Geological Map of Yugoslavia

Pomella H, Klötzli U, Scholger R, Stipp M, Fügenschuh B (2011) The Northern Giudicarie and the Meran-Mauls fault (Alps, Northern Italy) in the light of new paleomagnetic and geochronological data from boudinaged Eo-/Oligocene tonalities. Int J Earth Sci 579: 118-130, doi:10.1007/s00531-010-0612-4

Pomella H, Stipp M, Fügenschuh B (2012) Thermochronological record of thrusting and strike-slip faulting along the Giudicarie fault system (Alps, Northern Italy). Tectonophysics 579: 118-130

Ricou LE, Siddans AWB (1986) Collision tectonics in thewestern Alps. Geol Soc Lond Spec Publ 19: 229–244, doi:10.1144/GSL.SP.1986.019.01.13

Rosenbaum G, Lister GS, Duboz C (2002) Reconstruction of the tectonic evolution of the western Mediterranean since the Oligocene. Journal of the Virtual Explorer 8: 107–126

Rosenberg CL (2004) Shear zones and magma ascent: A model based on a review of the Tertiary magmatism in the Alps. Tectonics 23: TC3002, doi:10.1029/2003TC001526

Rosenberg CL, Berger A (2009) On the causes and modes of exhumation and lateral growth of the Alps. Tectonics 28: doi:10.1029/2008TC002442

Rosenberg CL, Kissling E (2013) 3D insight into Central Alpine Collision: lower plate or upper plate indentation? Geology 41: 1219-1222

Săndulescu M, Kräutner HG, Balintoni I, Russo-Săndulescu D, Micu M (1981a) The Structure of the East Carpathians, Guide Book to Excursion B1 of the Carpatho-Balkan Geological Association 12th Congress, Bucharest, pp 1–92

Scharf A, Handy MR, Favaro S, Schmid SM, Bertrand A (2013) Modes of orogen-parallel stretching and extensional exhumation in response to plate indentation and roll-back subduction (Tauern Window, Eastern Alps). Int J Earth Sci 102(6): 1627-1654, 10.1007/s00531-013-0894-4

Schefer S, Cvetković V, Fügenschuh B, Kounov A, Ovtcharova M, Schaltegger U, Schmid SM (2011) Cenozoic granitoids in the Dinarides of southern Serbia: age of intrusion, isotope geochemistry, exhumation history and significance for the geodynamic evolution of the Balkan Peninsula. Int J Earth Sci 100: 1181–1206, doi: 10.1007/s00531-010-0599-x

Schettino A, Turco E (2006) Plate kinematics of the Western Mediterranean region during the Oligocene and Early Miocene. Geophys J Int 166: 1398–1423

Schiunnach D, Scardia G, Tremolada F, Solva IP, et al. (2010) The Monte Orfano Conglomerate revisited: stratigraphic constraints on Cenozoic tectonic uplift of the Southern Alps (Lombardy, northern Italy). Int J Earth Sci 99: 1335-1355

Schlunegger F, Matter A, Burbank DW, Klaper EM, (1997) Magnetostratigraphic constraints on relationships between evolution of the central Swiss Molasse basin and Alpine orogenic events. Geol Soc Am Bull 109(2): 225-241

Schmid SM, Slejko D (2009) Seismic source characterization of the Alpine foreland in the context of a probabilistic seismic hazard analysis by PEGASOS Expert Group 1 (EG1a). Swiss J Geosci 102: 121–148.

Schmid SM, Aebli HR, Heller F, Zingg A (1989) The role of the Periadriatic Line in the tectonic evolution of the Alps. Geol Soc Lond Spec Publ 45: 153-171

Schmid SM, Bernoulli D, Fügenschuh B, Matenco L, Schefer S, Schuster R, Tischler M, Ustaszewski K (2008) The Alpine-Carpathian-Dinaridic orogenic system: correlation and evolution of tectonic units. Swiss J Geosci 101: 139-183

Schmid SM, Fügenschuh B, Kissling E, Schuster R (2004) Tectonic map and overall architecture of the Alpine orogen. Eclogae Geol Helv 97: 93–117; Brief description of recent changes applied in November 2006 to Tectonic map of the Alps as published by Schmid et al. 2004.

Schmid SM, Kissling E (2000) The arc of the western Alps in the light of geophysical data on deep crustal structure. Tectonics 19(1): 62–85

Schmid SM, Pfiffner OA, Froitzheim N, Schönborn G, Kissling E (1996) Geophysical-geological transect and tectonic evolution of the Swiss-Italian Alps. Tectonics 15(5): 1036-1064

Schmid SM, Scharf A, Handy MR, Rosenberg CL (2013) The Tauern Window (Eastern Alps. Austria): a new tectonic map, with cross-sections and a tectonometamorphic synthesis. Swiss J Geosci 106: 1-32

Schneider S, Rosenberg CL, Scharf A, Hammerschmidt K (submitted) Translation of indentation into lateral extrusion across a restraining bend: The western Tauern Window, Eastern Alps. Tectonics

Schönborn G (1992) Alpine tectonics and kinematic models of the central Southern Alps. Mem Sci Geol Univ Padova XLIV: 229-393

Schönborn G (1999) Balancing cross sections with kinematic constraints: The Dolomites (nothern Italy). Tectonics 18(3): 527-545

Schumacher ME, Laubscher HP (1996) 3D crustal architecture of the Alps-Apennines join - a new view on seismic data. Tectonophysics 260: 349-363

Seghedi I, Downes H, Szakacs A, Mason PRD, Thirlwall MF, Rosu E, Pecskay Z, Márton E, Panaiotu C (2004) Neogene-Quaternary magmatism and geodynamics in the Carpathian-Pannonian region: a synthesis. Lithos 72: 117–146

Séranne M (1999) The Gulf of Lion continental margin (NW Mediterranean) revisited by IBS: an overview. Geol Soc Lond Spec Publ 156: 15–36

Soták J, Biron A, Dunkl I, Prokesova R, Magyar J, Rudinec R, Spišiak J (1999) Alpine Penninics in the Eastern Slovakia: from crustal updoming to basin downfaulting. Geologica Carpathica 50: 172–174

Spada M, Bianchi I, Kissling E, Agostinetti P, Wiemer S (2013) Combined controlled-source seismology and receiver function information to derive 3D-Moho topography for Italy. Geophys J Int: doi:10.1093/gji/ggt148

Spakman W, Wortel MJR (2004) A tomographic view on Western Mediterranean geodynamics. Chapter 2. In: Cavazza W, Roure FM, Stampfli GM, Ziegler PA (eds) The Transmed Atlas—The Mediterranean Region from Crust to Mantle. Springer, Berlin, pp 31–52

Stampfli GM, Borel GD (2002) A plate tectonic model for the Paleozoic and Mesozoic constrained by dynamic plate boundaries and restored synthetic oceanic isochrones. Earth Planet Sci Lett 196: 17–33

Stampfli GM, Hochard C (2002) Plate tectonics of the Alpine realm. Geol Soc Lond Spec Publ 327: 89–111

Sue C, Tricart P (2003) Neogene to ongoing normal faulting in the inner western Alps: A major evolution of the late Alpine tectonics. Tectonics 22(5): 1050-1075

Šušnar M, Bukovac J (1978) Sheet "Drvar", 1:100.000, Geological Map of Jugoslavia

Szentgyörgyi K (1989) Sedimentological and faciological characteristics of the Senonian pelagic formations of the Hungarian plain. Acta Geol Hung 32 (12): 107–116

Szepesházy K (1973) Upper Cretaceous and Paleogene formations of the northwest Tiszántú. l. Akadémiai Kiadó, Budapest.

Tari GC (1996) Extreme crustal extension in the Rába river extensional corridor (Austria/Hungary). Mitteilungen der Gesellschaft der Geologie- und Bergbaustudenten in Österreich 41: 1–17

Tari V (2002) Evolution of the northern and western Dinarides: a tectonostratigraphic approach. EGU Stephan Mueller Special Publication Series 1: 223–236

Thomas JC, Claudel ME, Collombet M, Tricart P, Chauvin A, Dumont T (1999) First paleomagnetic data from the sedimentary cover of the French penninic Alps: Evidence for Tertiary counterclockwise rotations in the western Alps. Earth Planet Sci Lett 171: 561 – 574, doi:10.1016/S0012-821X(99)00182-X

Tischler M (2005) A combined structural and sedimentological study of the Inner Carpathians at the northern rim of the Transylvanian basin (N. Romania). Unpublished Ph.D. Thesis, Universität Basel, Basel, Switzerland

Tischler M, Gröger HR, Fügenschuh B, Schmid SM (2007) Miocene tectonics of the Maramures area (Northern Romania): implications for the Mid-Hungarian fault zone. Int J Earth Sci 96: 473–496

Tomljenović B, Csontos L, Márton E, Márton P (2008) Tectonic evolution of the northwestern Internal Dinarides as constrained by structures and rotation of Medvenica Mountains, North Croatia. Geol Soc Lond Spec Publ 298: 145-167

Torsvik TH, Müller DR, Van der Voo R, Steinberger B, Gaina C (2008) Global plate motion frames: toward a unified model. Reviews of Geophysics: 46 (RG3004/2008)

Turco E, Macchiavelli C, Mazzoli S, Schettino A, Pierantoni PP (2012) Kinematic evolution of Alpine Corsicia in the framework of Mediterranean mountain belts. Tectonophysics 579: 193-206

Ustaszewski K, Schmid SM (2006) Control of preexisting faults on geometry and kinematics in the northernmost part of the Jura fold-and-thrust belt. Tectonics 25: TC5003, doi:10.1029/2005TC001915

Ustaszewski K, Schmid SM (2007a) Latest Pliocene to recent thick-skinned tectonics at the Upper Rhine Graben – Jura Mountains junction. Swiss J Geosci 100: 293–312, DOI 10.1007/s00015-007-1226-0

Ustaszewski K, Schmid SM, Fügenschuh B, Tischler M, Kissling E, Spakman W (2008) A map-view restoration of the Alpine-Carpathian-Dinaridic system for the Early Miocene. Swiss J Geosci 101(1): 273-294

Ustaszewski K, Kounov A, Schmid SM, Schaltegger U, Krenn E, Frank W, Fügenschuh B (2010) Evolution of the Adria-Europe plate boundary in the northern Dinarides, From continent-continent collision to back-arc extension. Tectonics 29: TC6017, doi:10.1029/2010TC002668

van Hinsbergen DJJ, Langereis CJ, Meulenkamp JE (2005) Revision of the timing, magnitude and distribution of Neogene rotations in the western Aegean region. Tectonophysics 396: 1–34, doi:10.1016/j.tecto.2004.10.001

van Hinsbergen DJJ, Schmid SM, (2012) Map-view restoration of the Aegean back-arc. Tectonics 31: TC5005, doi:10.1029/2012TC003132

Vignaroli G, Faccenna C, Jolivet L., Piromallo C, Rossetti F (2008) Subduction polarity reversal at the junction between the Western Alps and the Northern Apennines, Italy. Tectonophysics 450: 34–50

Viola G, Mancktelow NS, Seward D (2001) Late Oligocene-Neogene evolution of Europe-Adria collision: New structural and geochronological evidence from the Giudicarie fault system (Italian Eastern Alps). Tectonics 20: 999 – 1020

Vrabec M, Pavlovcic Preseren P, Stopar B (2006) GPS study (1996-2002) of active deformation along the Periadriatic fault system in northeastern Slovenia: tectonic model. Geol Carpath 57(1): 57-65

Viti M, Mantovani E, Babbucci D, Tamburelli C (2009) Generation Of Trench-Arc-Back Arc Systems In The Western Mediterranean Region Driven By Plate Convergence. Ital J Geosci (Boll Soc Geol It) 128 (1): 89-106

von Blanckenburg F, Davies JH (1995) Slab breakoff: A model for syncollisional magmatism and tectonics in the Alps. Tectonics 14(1): 120-131

von Hagke C, Cederboom CE, Oncken O, Stöckli DF, Rahn MK (2012) Linking the northrn Alps with their foreland: The latest exhumation history resolved by low-temperature thermochronology. Tectonics 31: TC5010, doi:1029/2011TC003078

Ward S (1994) Constraints on the seismotectonics of the central Mediterranean from very long baseline interferometry. Geophys J Int 11: 441– 452

Zhu H, Bozdag E, Peter D, Tromp J (2012) Structure of the European upper mantle revealed by adjoint tomography. Nature Geoscience 5: 493-498

Zingg A, Handy MR, Hunziker JC, Schmid SM (1990) Tectonometamorphic history of the Ivrea Zone and its relation to the crustal evolution of the Southern Alps. Tectonophysics 182: 169–192

Figure Captions

Figure A1: Compilation of post-Eocene shortening and extension in the Alps: **(a)** Displacements from 20 Ma to present**; (b)** Displacements from 34 to 20 Ma. Map colours show paleogeographic affinity of main tectonic units in the Alps as modified from Schmid et al. (2004, with corrections), Froitzheim et al. (1996) and Handy et al. (2010). Arrows connect present locations of deformed markers (tips) with original, retrodeformed locations (dots) in a 2-D, map-view displacement field. Arrows connected to a short bar indicate the amount of shortening in a cross section as measured from the tip line of the thrust to the end of the section. References: Gratier et al. 1989, Philippe et al. 1996, Burkhard and Sommaruga 1989, Burkhard 1990, Frisch et al. 1998, Fügenschuh et al. 1997, Gouffon 1993, Grasemann and Mancktelow 1993, Handy et al. 2010, Hitz and Pfiffner 1995, Kempf and Pfiffner 2004, Pfiffner 2009, Lickorish and Ford 1998, Milnes 1978, Nussbaum 2000, Scharf et al. 2013, Schmid et al. 1996, Schönborn 1992, 1999, Tari 1996.

Figure A2: Major fault systems in the Alps and their division into segments for restoration. European coastline and cities shown for reference: L = Lyon, Z = Zürich, M = Munich, W = Vienna, G = Genoa.

Figure A3: Straight segments of fault systems used to restore the Alps. Red points are identical to those shown in Fig. **A2**.

Figure A4: Restoration of the Jura fold-and-thrust belt (step 1). Thin black lines represent present-day outline of the frontal thrusts in the Alps. Gray line is the present European coastline.

Figure A5: Restoration of the Subalpine Molasse and Châines Subalpines (step 2) Faults and coastlines as in Fig. **A4.**

Figure A6: Restoration of the Maritime Alpes Front (step 3). Thrusts and coastlines as in Fig. **A4.**

Figure A7: Restoration of Giudicarie strike-slip motion and Penninic N-S shortening in step 4. Thrusts and coastlines as in Fig. **A4.**

Figure A8: Restoration of S-directed thrusting in the Southern Alps in step 5. Thrusts and coastlines as in Fig. **A4.**

Figure A9: Total translation (steps 1-4) and clockwise backrotation about Ivrea (step 5) of the Adriatic Plate to its position at 20 Ma.

Figure A10: Restoration of Insubric strike-slip motion (purple), internal Penninic deformation (purple) and the Helvetic thrusting (blue) in step 6.

Figure A11: Restoration of the Western Alpine Arc (step 7). Location of the Corsica-Sardinia block at 35 Ma is taken from Dewey et al. (1989). Note the different positions of their and our rotational poles for the same rotation! Position of faults and Adriatic coastline at 35 Ma taken from Fig. **A10**. European coastline, cities and present thrust front in Alps and Carpathians as in Fig. **A2.**

Figure B1: Horizontal tomographic depth slices of Lippitsch et al. (2003, their Figs. 12c, e, f) with major Alpine surface structures shown for reference: (a) 150 km; (b) 210 km; (c) 240 km. The 4% contours of the upper surfaces of the positive (blue) anomalies were used for the contours in Fig. **B3**. Major Alpine structures: AF = Alpine thrust front, PF = Periadriatic Fault (dashed).

Figure B2: Tomographic cross sections for traces shown in the map inset: (a) SE-dipping slab beneath the Central Alps; (b) Short subvertically dipping slab along the TRANSALP section discussed in text; (c) Eastern Alps slab beneath the Tauern Window; (d) Eastern Alps slab beneath the Eastern Alps. Note that sections (c) and (d) are oriented oblique to the rotational axis of the Eastern Alps slab as shown in Fig. **B3**. The slab dip in (c) and (d) is therefore apparent. Map view and cross sections in (a), (c) and (d) are modified from Lippitsch et al. (2003, their figs. 12, 13b, c) and the TRANSALP section in (d) is based on results of Lippitsch et al. (2003) as published in Kissling et al. (2006, their fig. 14c), with the Moho modified from Lüschen et al. (2004) and Kummerow et al. (2004).

Figure B3: Backrotation of slab anomalies beneath the Western and Central Alps (blue) and Eastern Alps (red). Thin coloured lines = depth contours (km) of upper surfaces of slab anomalies in Fig. **B1** projected to the surface. Dashed lines = traces of tomographic cross sections in Fig. **B2**. Thick coloured lines = backrotated positions of leading edges of slabs. Arrows perpendicular to the rotation axes (slab hinges) indicate amount and direction of backrotation, as discussed in text. Dotted lines show coastlines for reference. Thin black lines show outlines of main thrust fronts in the Alps.

Figure B4: Miocene retrotranslation of the horizontalized Western Alps slab; Miocene retrotranslation (blue) and backrotation (red) of the horizontalized Eastern Alpine (Adriatic) slab to its location at 20 Ma (Fig. **10** in main text). Retrotranslation vector (blue arrow): 113 km to S55°E. Backrotation angle (red) = 20° Dotted lines = coastlines for reference, thin black lines = main thrust fronts in the Alps.

Figure B5: 20-35 Ma retrotranslation of the horizontalized Eastern Alps slab to its location at 35 Ma (Fig. **8** in main text). Retrotranslation vector (blue arrow): 200 km to S123°E. Dotted lines = coastlines for reference, thin black lines = main thrust fronts in the Alps.

Figure B6: 35-67 Ma retrotranslation of the horizontalized Eastern Alps slab to its location at 67 Ma (Fig. **6** in main text). Retrotranslation vector: 465 km to S150°E (Handy et al. 2010, their table 1). Dotted lines = coastlines for reference, thin black lines = main thrust fronts in the Alps.

Figure B7: Late Cretaceous retrotranslation of the Easterns slab to its location at 84 Ma at or just after the onset of subduction of Alpine Tethys (Fig. **5** in main text). Retrotranslation vector (blue arrow): 150 km to S150°E (Handy et al. 2010, their table 1). Dotted lines = coastlines for reference, thin black lines = main thrust fronts in the Alps.

Tables

Table A1: Faults, tectonic units and sources used in the map reconstructions.

Figure A1a

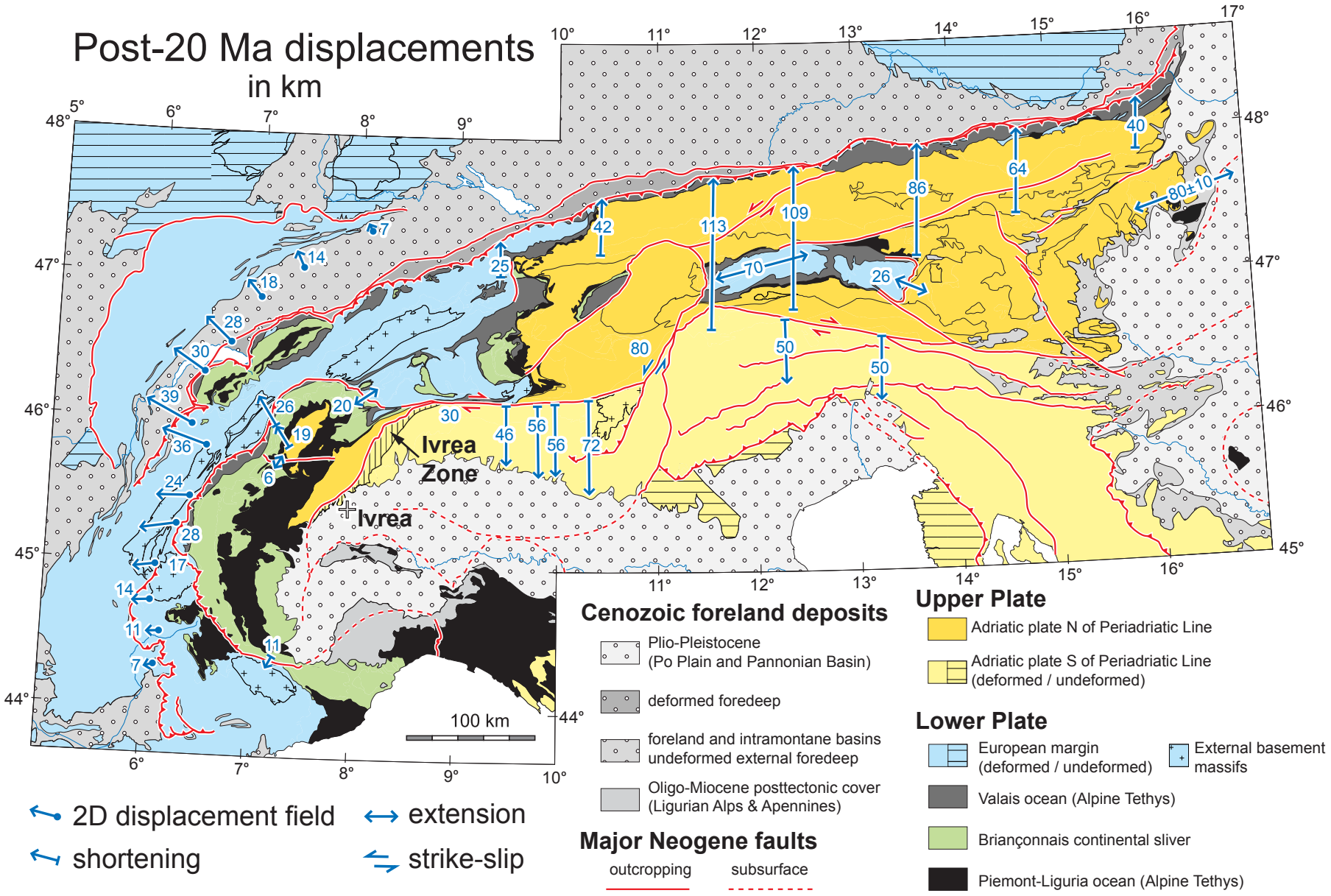
Post-20 Ma displacements
in km
Ivrea
Zone
Ivrea
100 km
2D displacement field
shortening
extension
strike-slip
Cenozoic foreland deposits
Plio-Pleistocene
(Po Plain and Pannonian Basin)
deformed foredeep
foreland and intramontane basins
undeformed external foredeep
Oligo-Miocene posttectonic cover
(Ligurian Alps & Apennines)
Major Neogene faults
outcropping
subsurface
Upper Plate
Adriatic plate N of Periadriatic Line
Adriatic plate S of Periadriatic Line
(deformed / undeformed)
Lower Plate
European margin
(deformed / undeformed)
External basement
massifs
Valais ocean (Alpine Tethys)
Briançonnais continental sliver
Piemont-Liguria ocean (Alpine Tethys)

Figure A1b

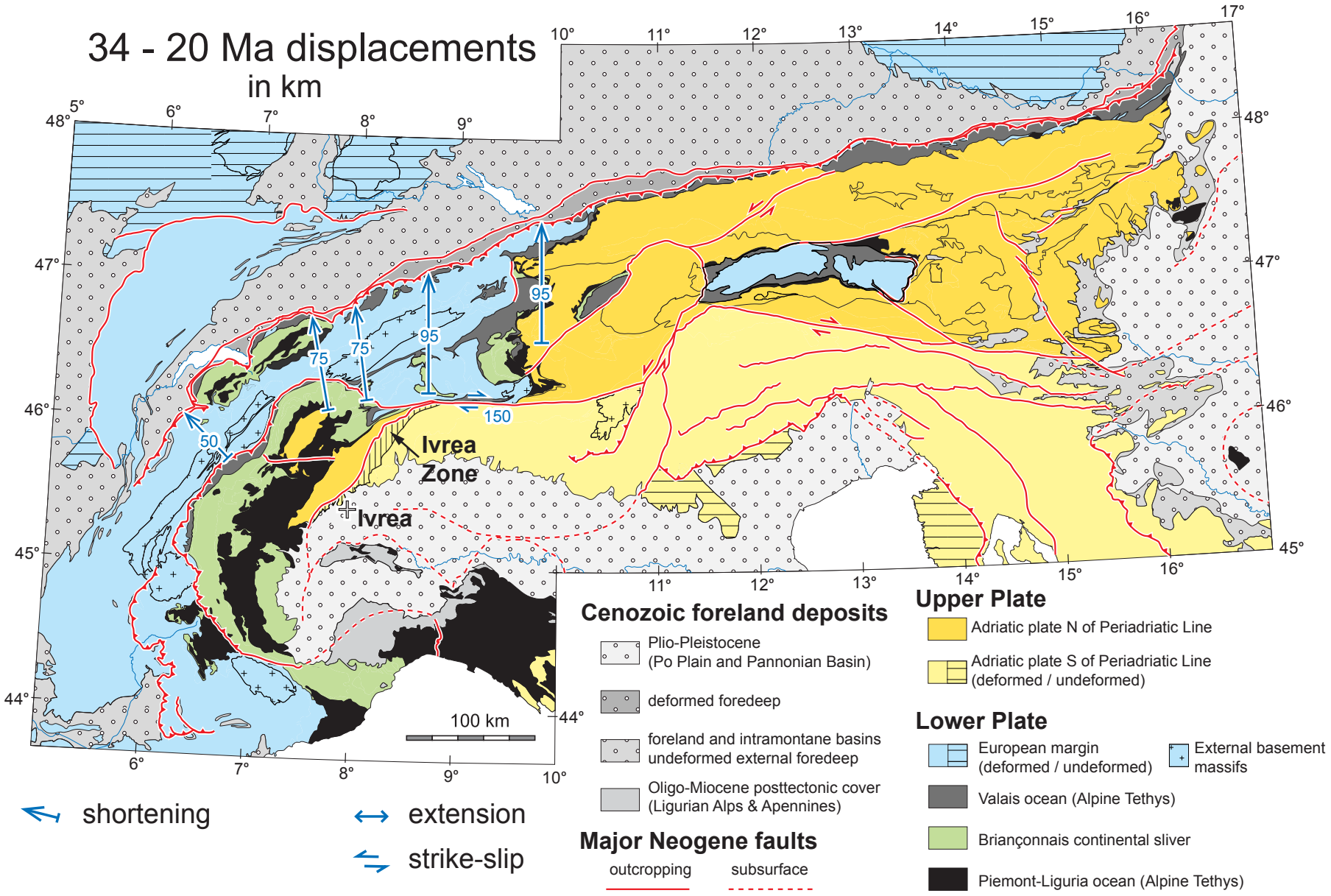
34 - 20 Ma displacements
in km
95
75
75
95
150
50
Ivrea
Zone
Ivrea
100 km
shortening
extension
strike-slip
Cenozoic foreland deposits
Plio-Pleistocene
(Po Plain and Pannonian Basin)
deformed foredeep
foreland and intramontane basins
undeformed external foredeep
Oligo-Miocene posttectonic cover
(Ligurian Alps & Apennines)
Major Neogene faults
outcropping
subsurface
Upper Plate
Adriatic plate N of Periadriatic Line
Adriatic plate S of Periadriatic Line
(deformed / undeformed)
Lower Plate
European margin
(deformed / undeformed)
External basement
massifs
Valais ocean (Alpine Tethys)
Briançonnais continental sliver
Piemont-Liguria ocean (Alpine Tethys)

Figure A2

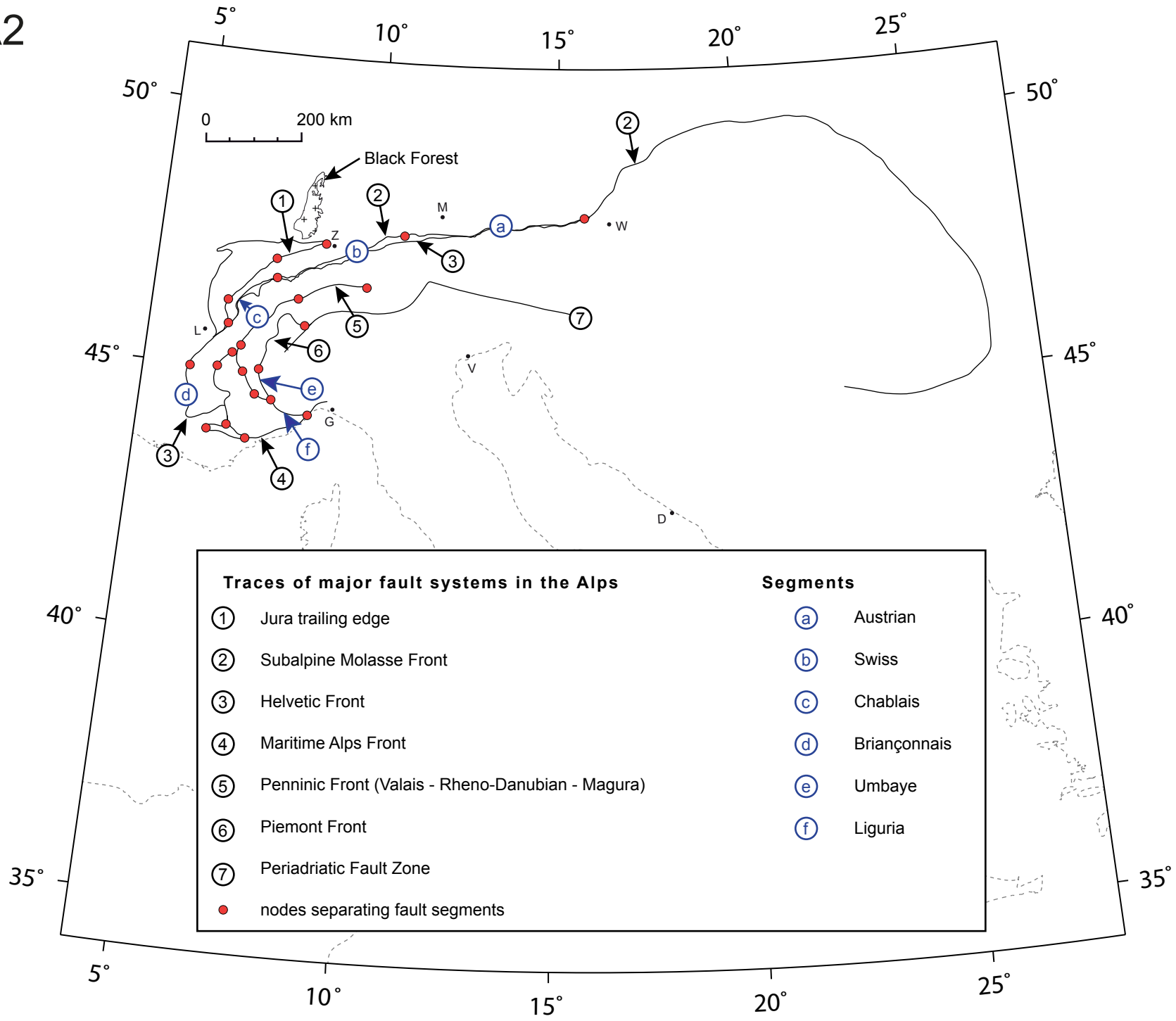
5°
10°
15°
20°
25°
50°
45°
40°
35°
0
200 km
Black Forest
M
W
Z
L
V
G
D
Traces of major fault systems in the Alps
1 Jura trailing edge
2 Subalpine Molasse Front
3 Helvetic Front
4 Maritime Alps Front
5 Penninic Front (Valais - Rheno-Danubian - Magura)
6 Piemont Front
7 Periadriatic Fault Zone
nodes separating fault segments
Segments
a Austrian
b Swiss
c Chablais
d Briançonnais
e Umbaye
f Liguria

Figure A3

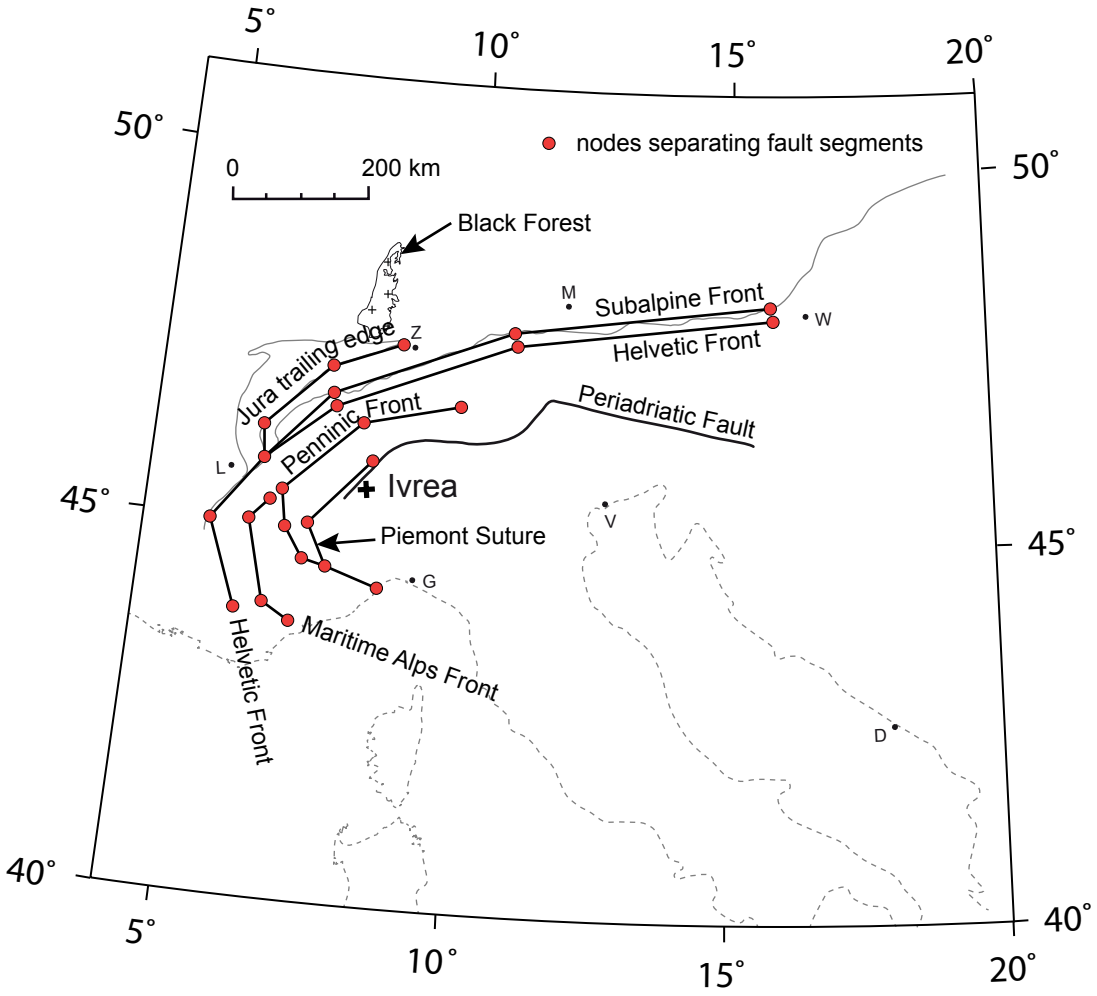
5°
10°
15°
20°
50°
45°
40°
nodes separating fault segments
0
200 km
Black Forest
Subalpine Front
Helvetic Front
Jura trailing edge
Penninic Front
Periadriatic Fault
Ivrea
Piemont Suture
Maritime Alps Front
Helvetic Front
M
W
Z
L
V
G
D

Figure A4

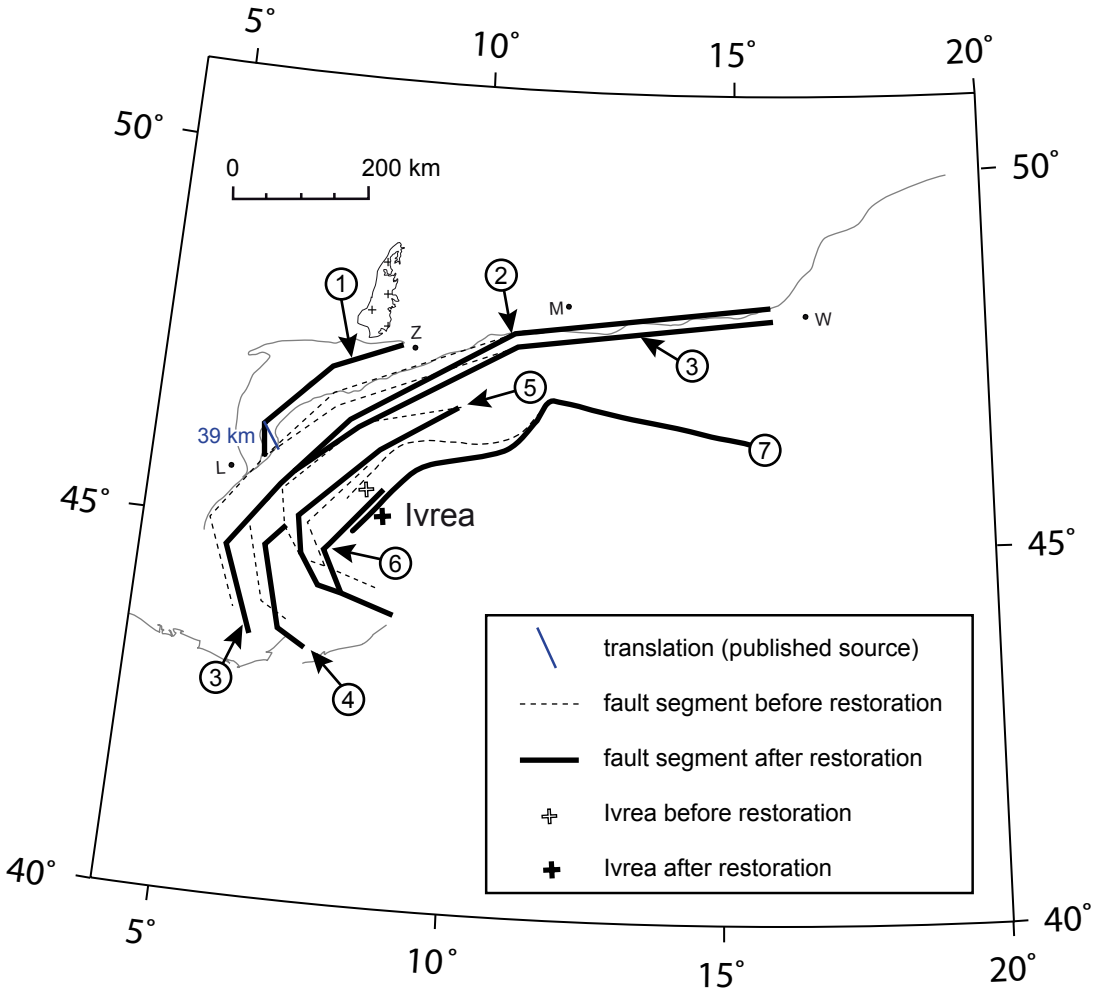

Step 1: restoration of Jura thrust belt

Figure A5

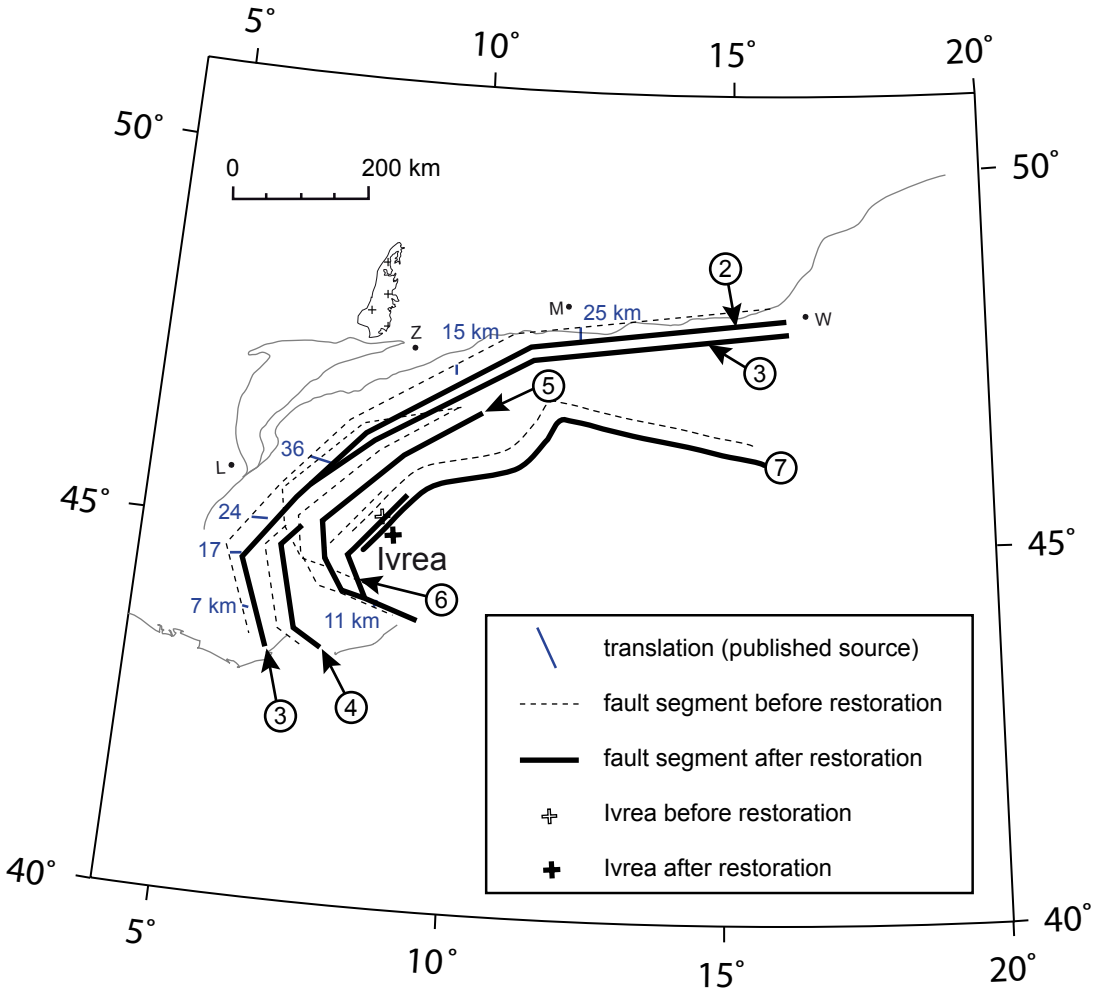

Step 2:
restoration of Subalpine Molasse, Chaines Subalpines, Maritimes Alpes fronts

Figure A6

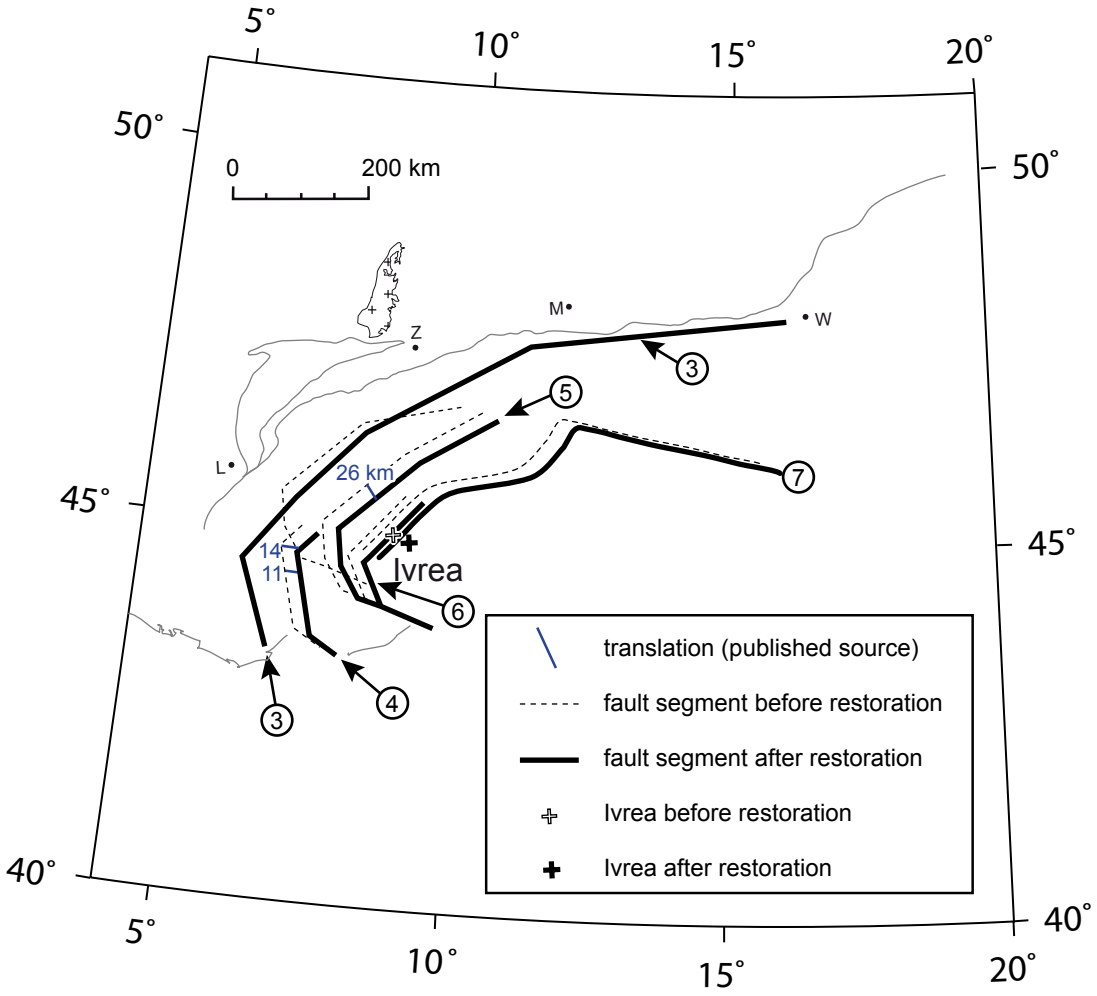

Step 3:
restoration of Maritimes Alpes and Penninic Front

Figure A7

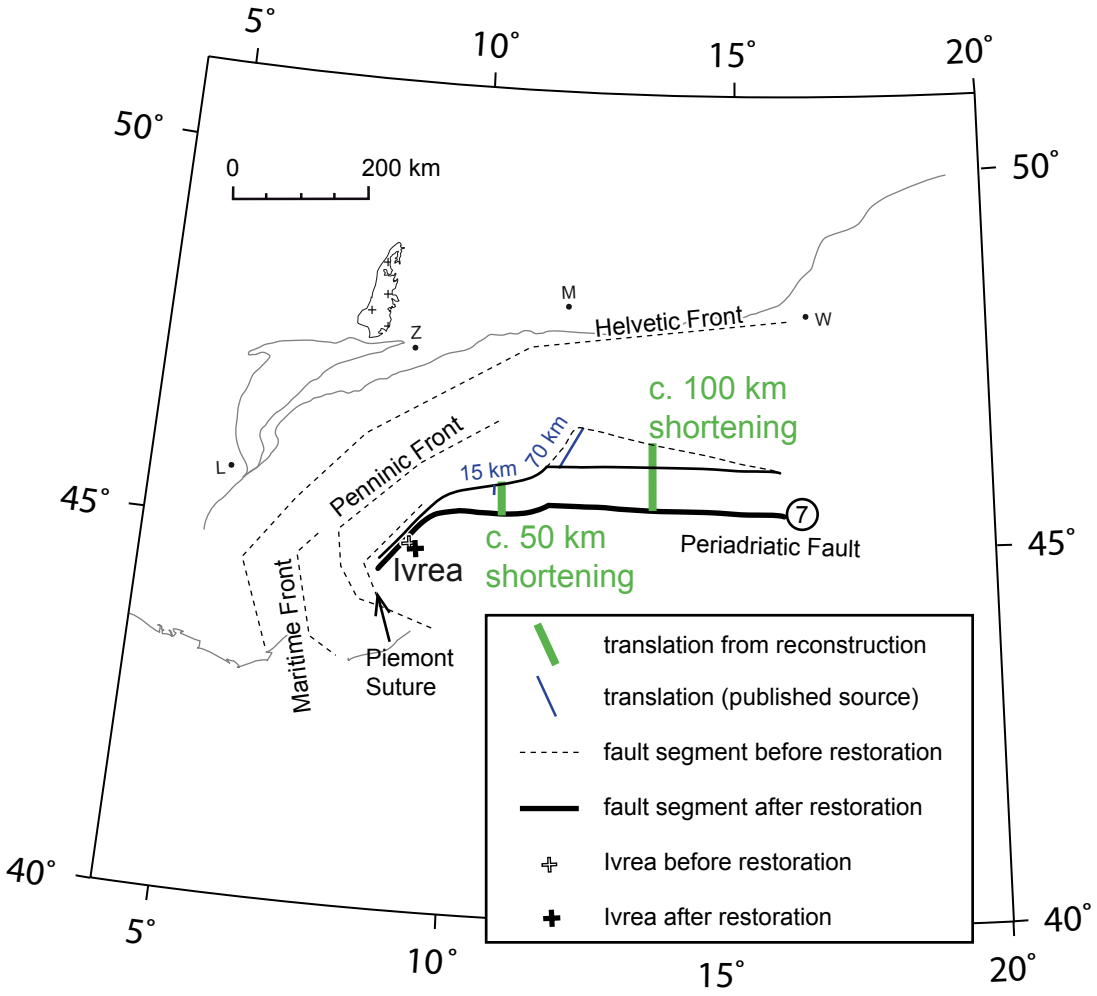

Step 4:
restoration of Giudicarie Line and internal Penninic shortening

Figure A8

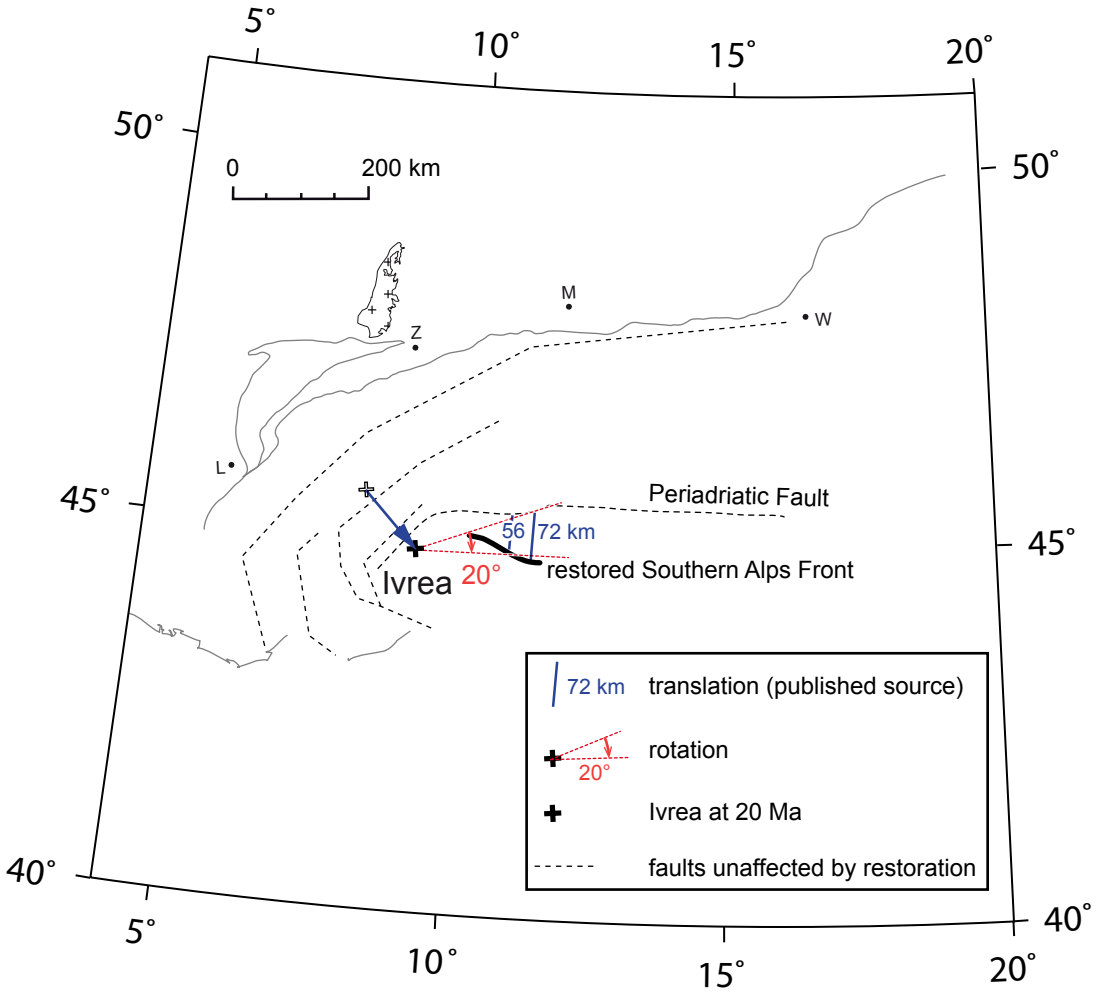

Step 5:
restoration of Southern Alps Front

Figure A9

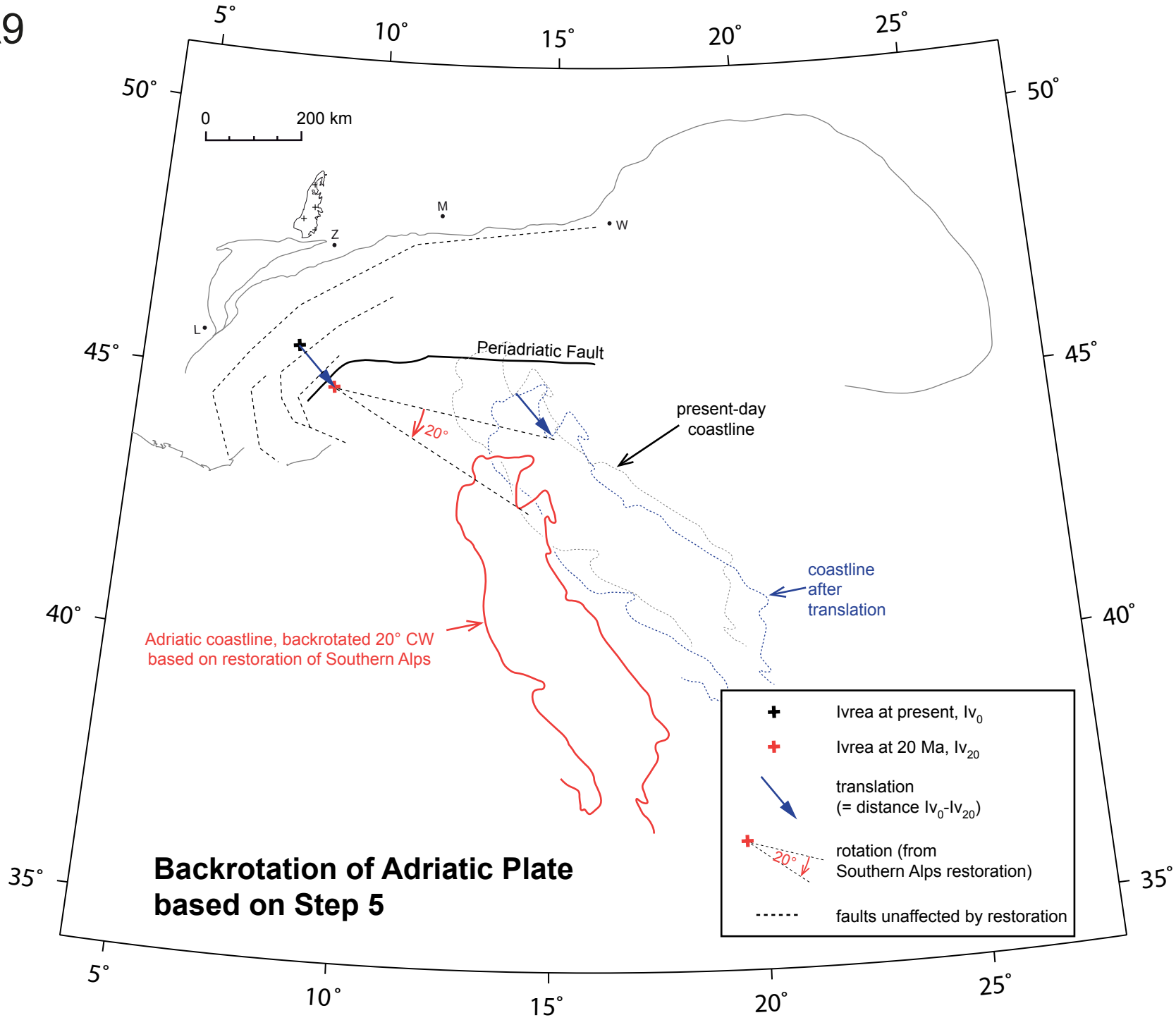
5°
10°
15°
20°
25°
50°
45°
40°
35°
0
200 km
M
W
Z
L
Periadriatic Fault
20°
present-day
coastline
coastline
after
translation
Adriatic coastline, backrotated 20° CW
based on restoration of Southern Alps
Ivrea at present, Iv0
Ivrea at 20 Ma, Iv20
translation
(= distance Iv0-Iv20)
rotation (from
Southern Alps restoration)
faults unaffected by restoration
Backrotation of Adriatic Plate
based on Step 5

Figure A10

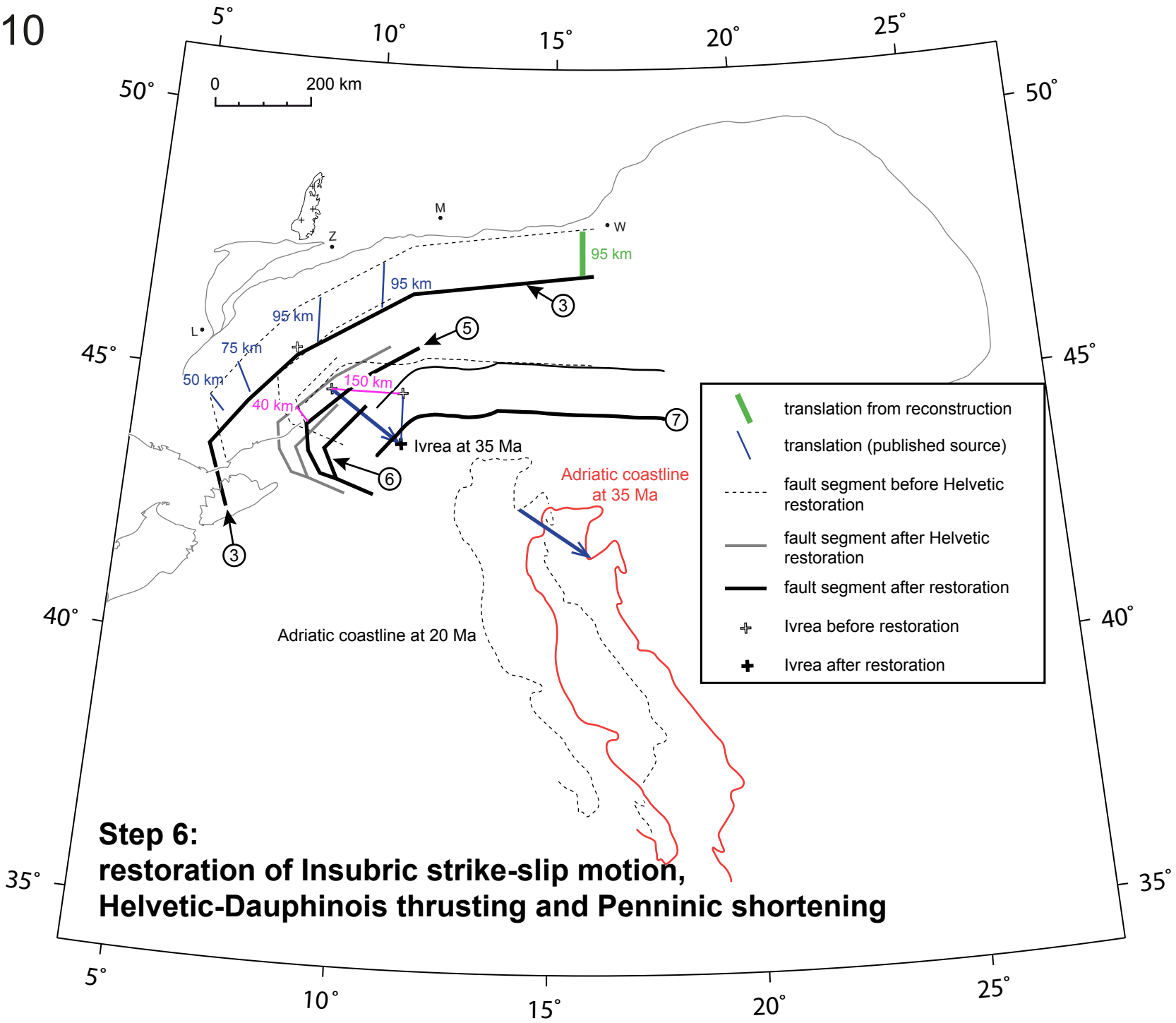
5°
10°
15°
20°
25°
50°
45°
40°
35°
0
200 km
M
Z
W
L
95 km
95 km
95 km
75 km
50 km
150 km
40 km
3
5
6
7
Ivrea at 35 Ma
Adriatic coastline at 35 Ma
Adriatic coastline at 20 Ma
translation from reconstruction
translation (published source)
fault segment before Helvetic restoration
fault segment after Helvetic restoration
fault segment after restoration
Ivrea before restoration
Ivrea after restoration
Step 6:
restoration of Insubric strike-slip motion,
Helvetic-Dauphinois thrusting and Penninic shortening

Figure A11

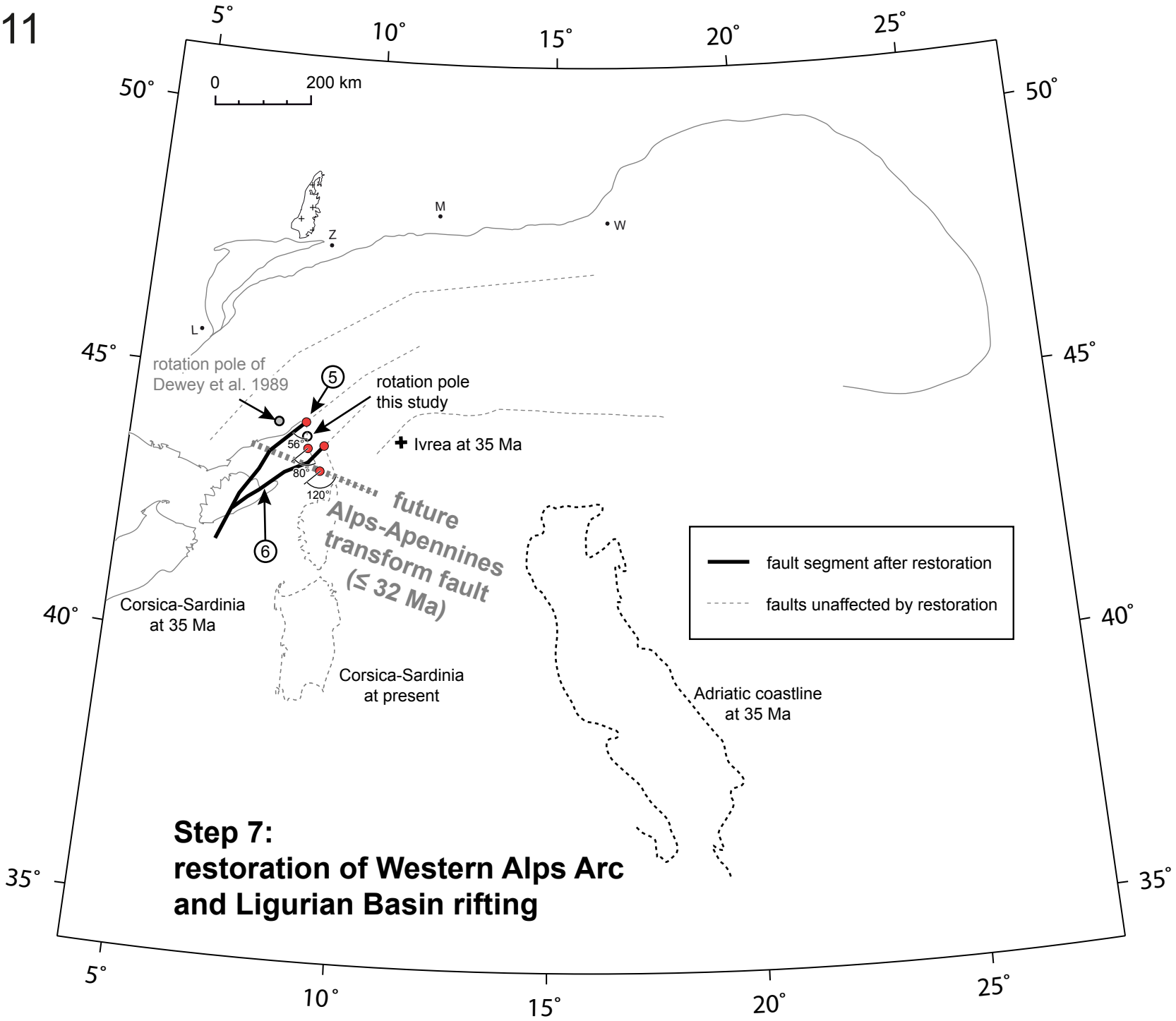
5°
10°
15°
20°
25°
50°
45°
40°
35°
0
200 km
M
W
Z
L
rotation pole of
Dewey et al. 1989
5
rotation pole
this study
Ivrea at 35 Ma
56°
80°
120°
6
future
Alps-Apennines
transform fault
(≤ 32 Ma)
Corsica-Sardinia
at 35 Ma
Corsica-Sardinia
at present
Adriatic coastline
at 35 Ma
fault segment after restoration
faults unaffected by restoration
Step 7:
restoration of Western Alps Arc
and Ligurian Basin rifting

Figure B1

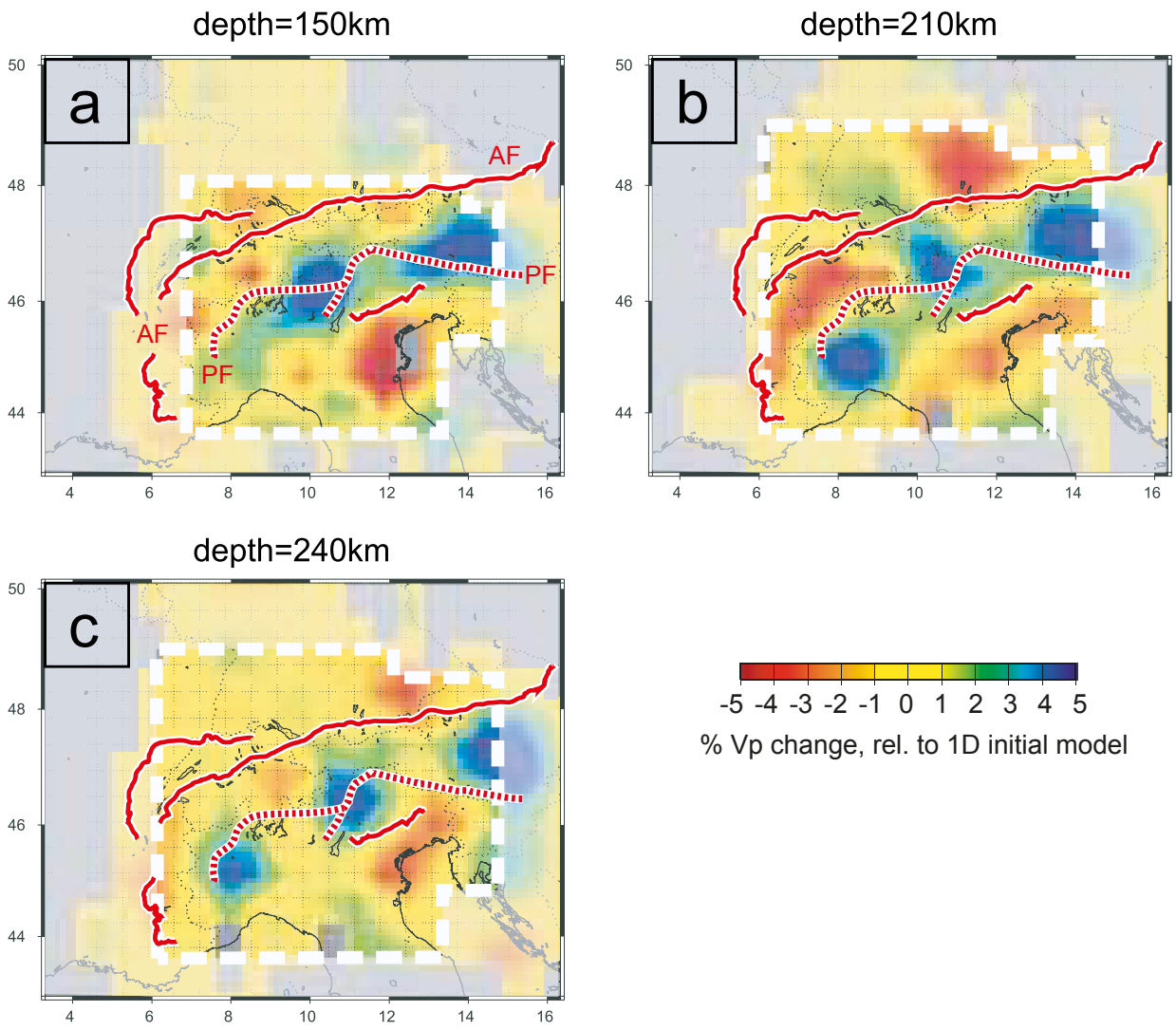
depth=150km
depth=210km
depth=240km
a
b
c
AF
PF
AF
PF
50
48
46
44
4
6
8
10
12
14
16
-5 -4 -3 -2 -1 0 1 2 3 4 5
% Vp change, rel. to 1D initial model

Figure B2

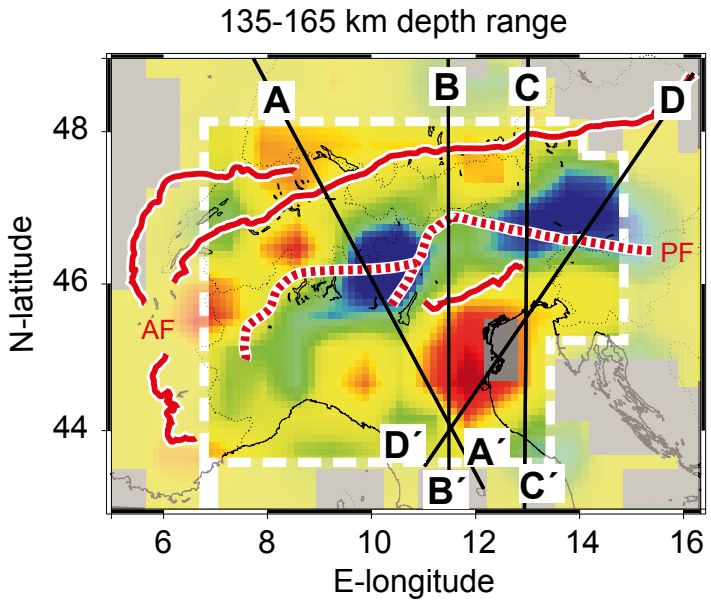

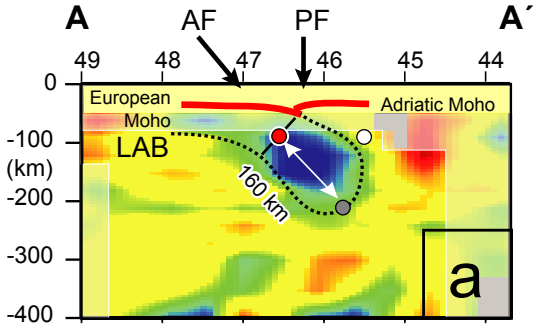

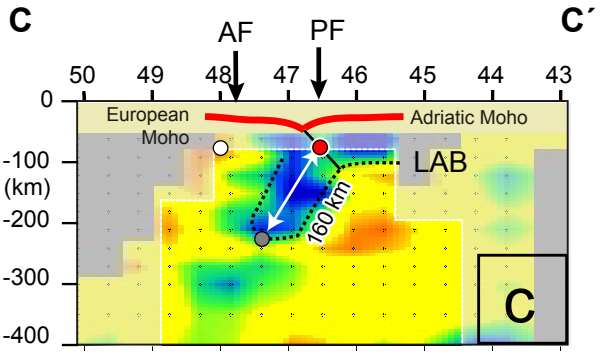

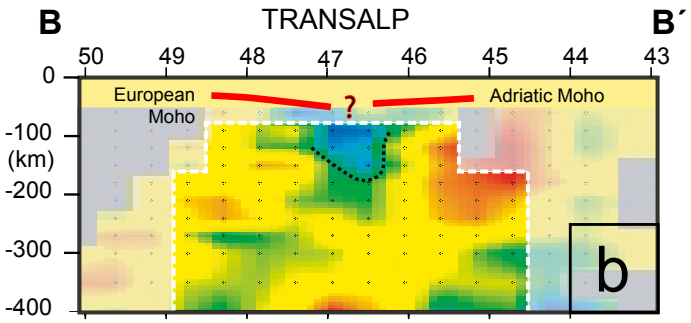

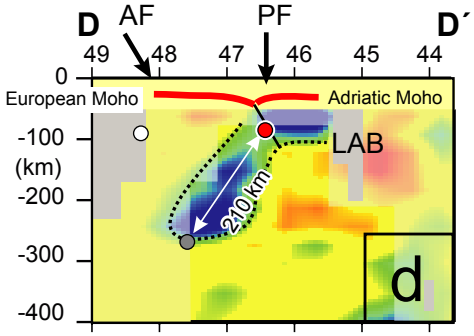

Scheme showing horizontalization of dipping slabs

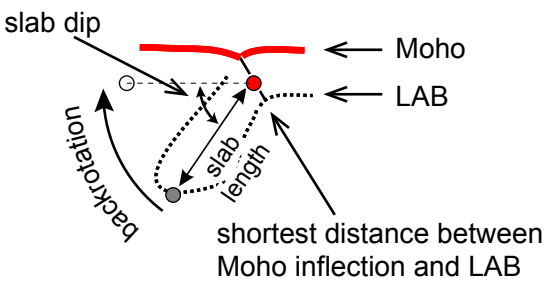

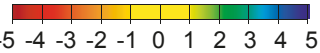

- rotation axis
- point on horizontalized leading edge of slab
- point on leading edge of dipping slab

Figure B3

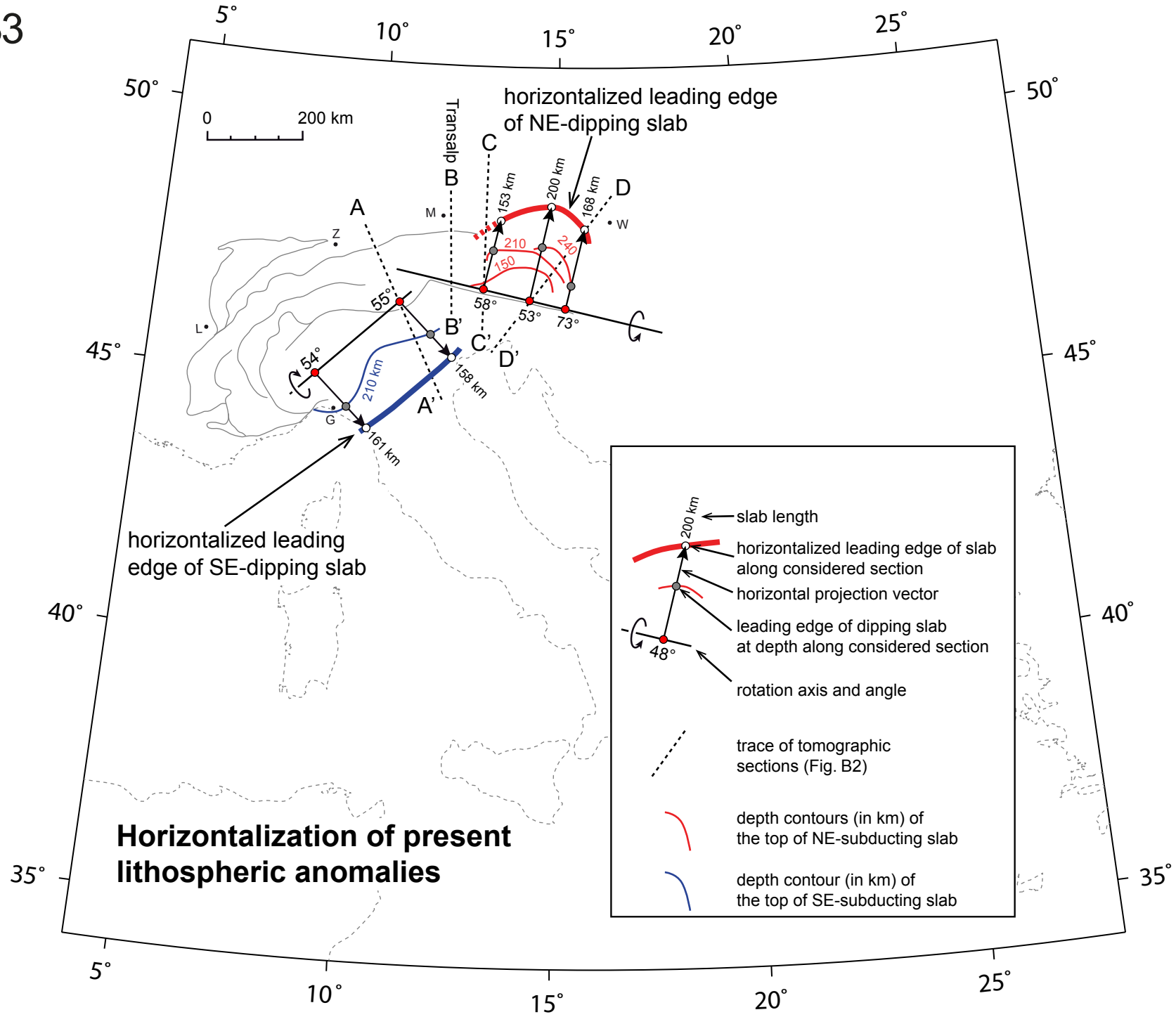
5°
10°
15°
20°
25°
50°
45°
40°
35°
0
200 km
Transalp
A
B
C
D
M
Z
L
G
W
A'
B'
C'
D'
153 km
200 km
168 km
210
240
150
58°
53°
73°
55°
54°
210 km
158 km
161 km
horizontalized leading edge of NE-dipping slab
horizontalized leading edge of SE-dipping slab
Horizontalization of present lithospheric anomalies
slab length
horizontalized leading edge of slab along considered section
horizontal projection vector
leading edge of dipping slab at depth along considered section
48°
rotation axis and angle
trace of tomographic sections (Fig. B2)
depth contours (in km) of the top of NE-subducting slab
depth contour (in km) of the top of SE-subducting slab

Figure B4

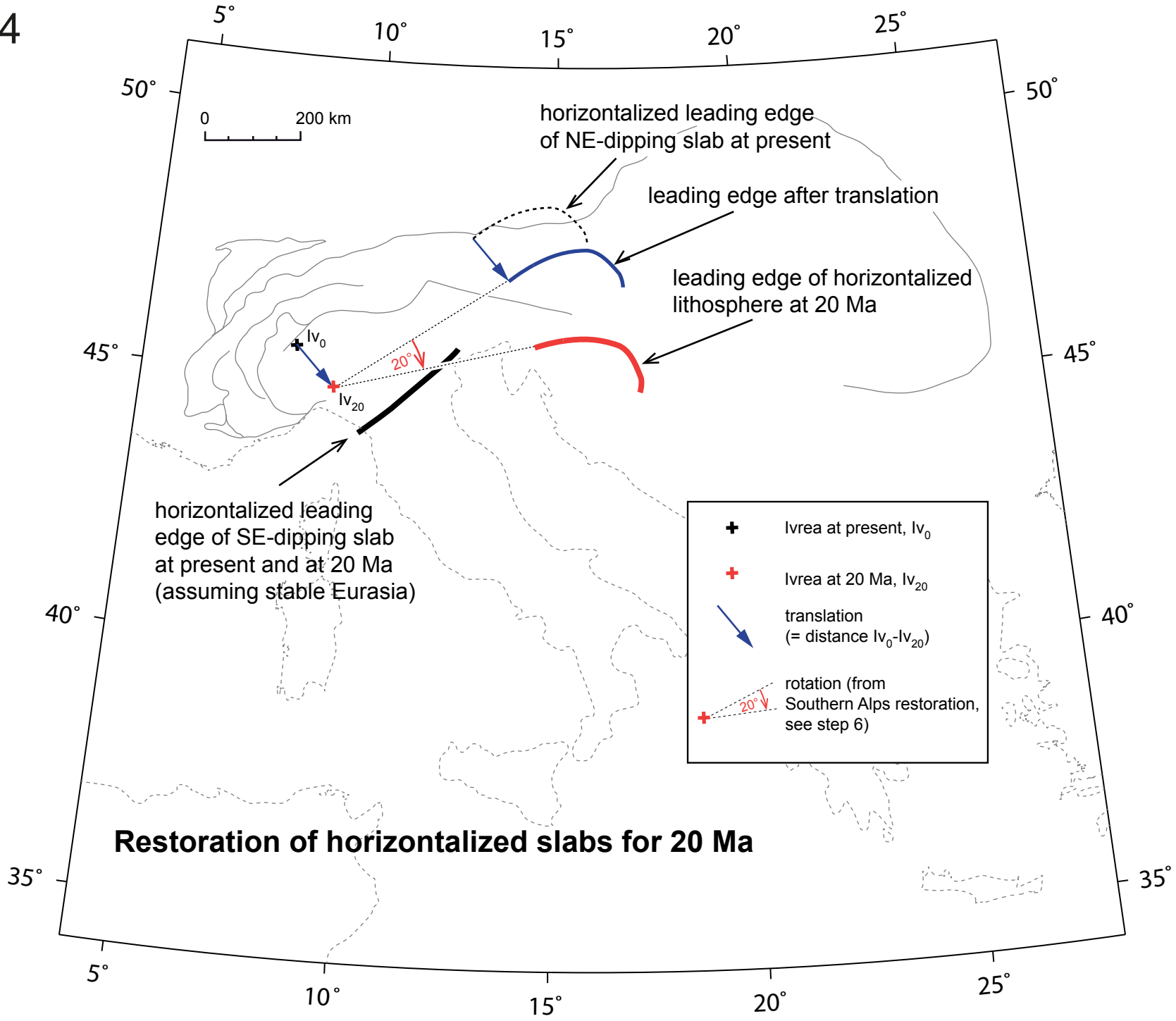
5°
10°
15°
20°
25°
50°
45°
40°
35°
0
200 km
horizontalized leading edge
of NE-dipping slab at present
leading edge after translation
leading edge of horizontalized
lithosphere at 20 Ma
Iv0
Iv20
20°
horizontalized leading
edge of SE-dipping slab
at present and at 20 Ma
(assuming stable Eurasia)
Ivrea at present, Iv0
Ivrea at 20 Ma, Iv20
translation
(= distance Iv0-Iv20)
rotation (from
Southern Alps restoration,
see step 6)
Restoration of horizontalized slabs for 20 Ma

Figure B5

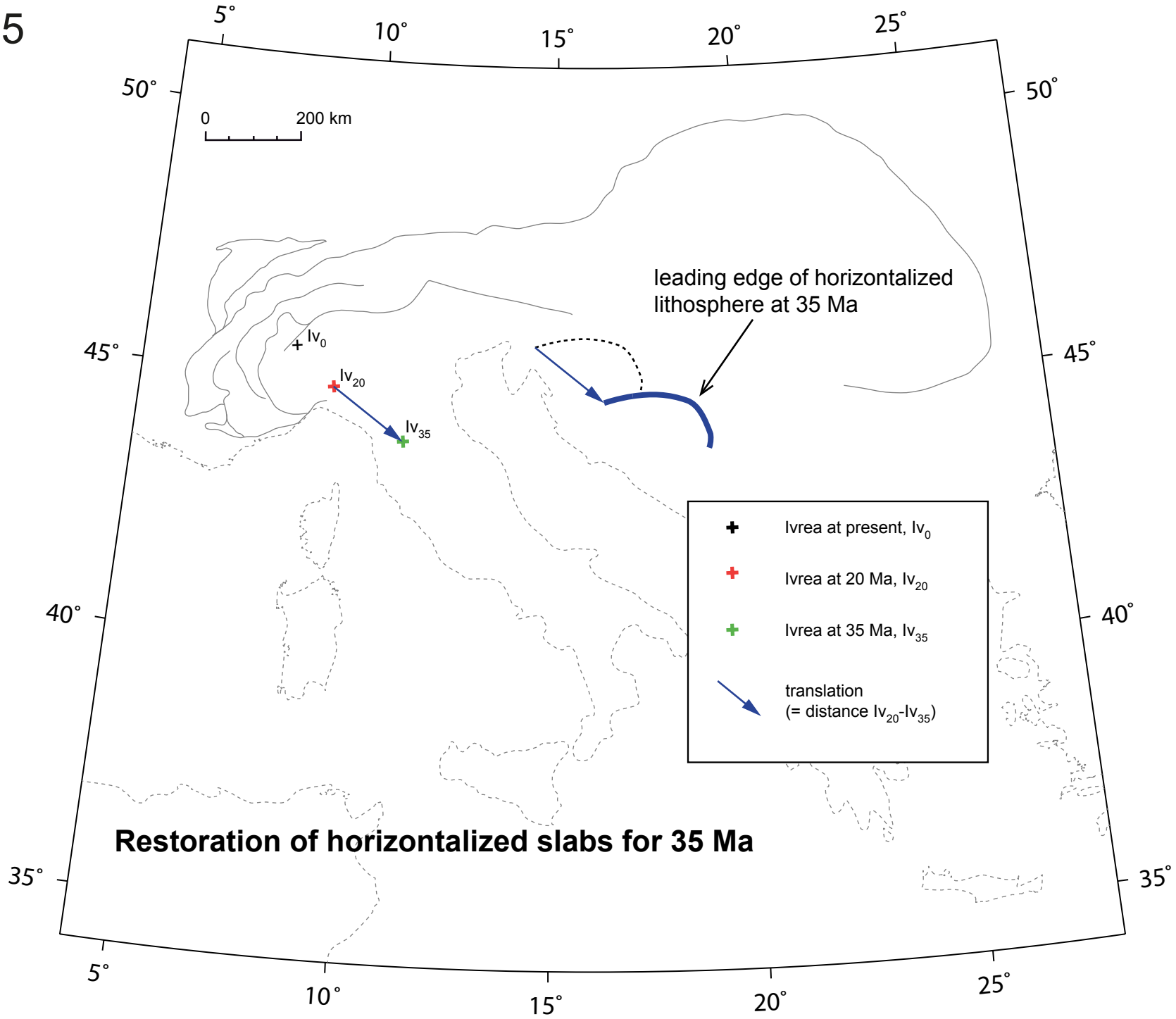
5°
10°
15°
20°
25°
50°
45°
40°
35°
0
200 km
leading edge of horizontalized lithosphere at 35 Ma
Iv0
Iv20
Iv35
Ivrea at present, Iv0
Ivrea at 20 Ma, Iv20
Ivrea at 35 Ma, Iv35
translation
(= distance Iv20-Iv35)
Restoration of horizontalized slabs for 35 Ma

Figure B6

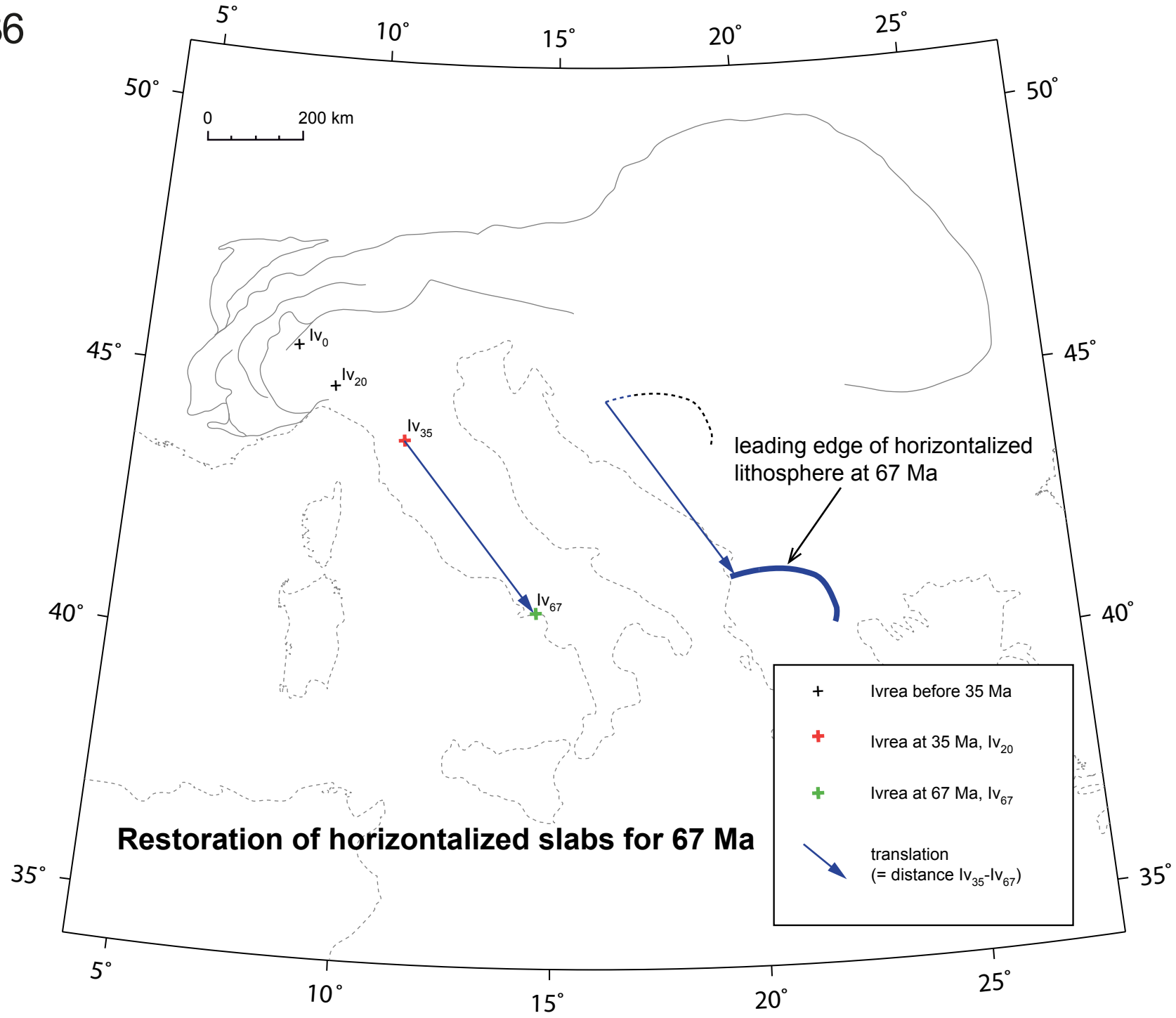
5°
10°
15°
20°
25°
50°
45°
40°
35°
0
200 km
Iv0
Iv20
Iv35
Iv67
leading edge of horizontalized lithosphere at 67 Ma
Restoration of horizontalized slabs for 67 Ma
Ivrea before 35 Ma
Ivrea at 35 Ma, Iv20
Ivrea at 67 Ma, Iv67
translation
(= distance Iv35-Iv67)

Figure B7

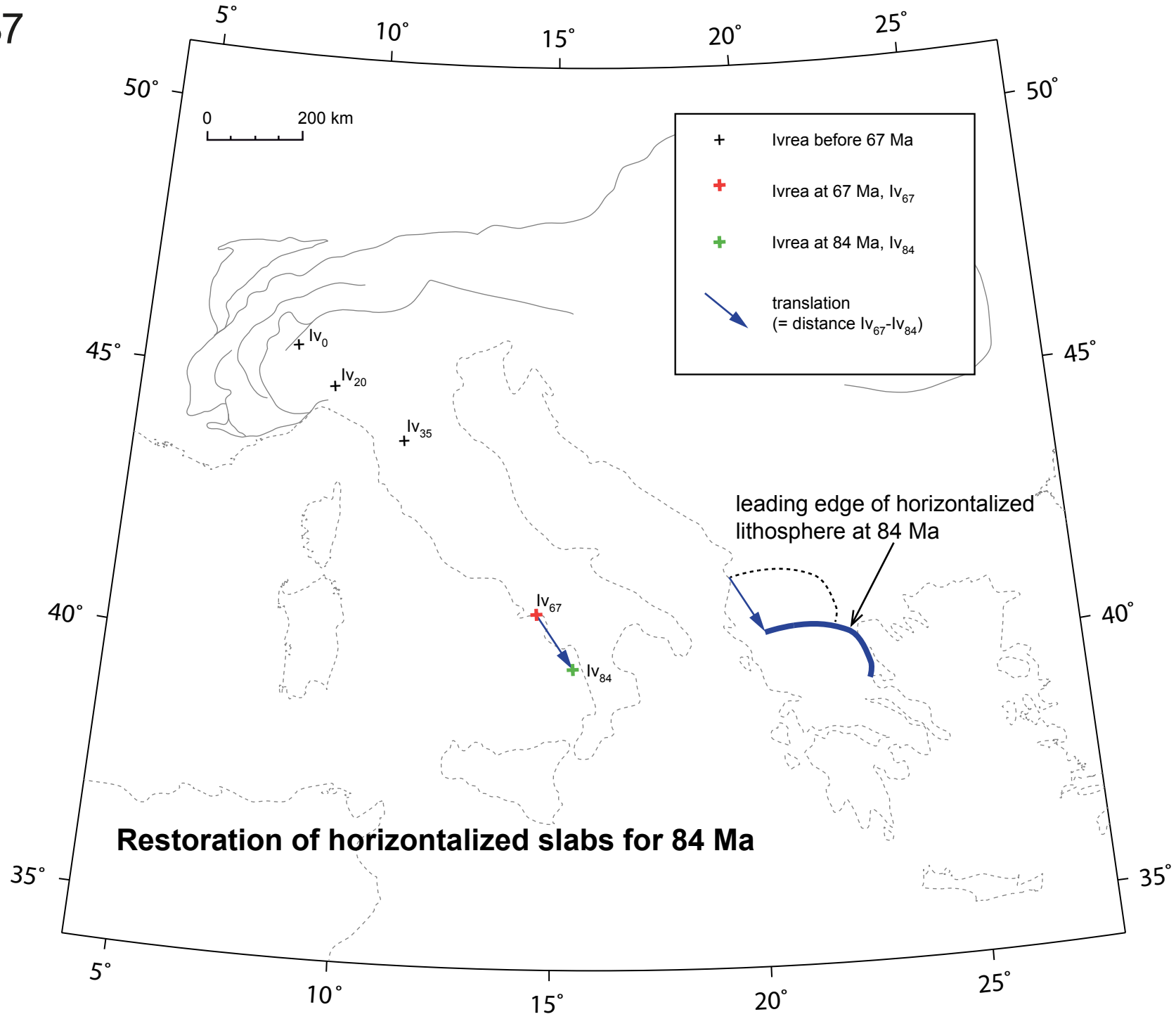
5°
10°
15°
20°
25°
50°
45°
40°
35°
0
200 km
Ivrea before 67 Ma
Ivrea at 67 Ma, Iv67
Ivrea at 84 Ma, Iv84
translation
(= distance Iv67-Iv84)
Iv0
Iv20
Iv35
Iv67
Iv84
leading edge of horizontalized
lithosphere at 84 Ma
Restoration of horizontalized slabs for 84 Ma

Table A1: Faults, tectonic units and sources used in the map reconstructions.

Faults used in reconstructions	Hangingwall units	Footwall units	References
Jura thrust-and-fold belt, trailing edge (JF)	Folded and thrusted Mesozoic	Mesozoic and Pliocene strata of the Plateau Jura	Becker 2000, Madritsch et al. 2008
East Vardar Obduction Front (EV)	East Vardar ophiolites	Dacia Mega-Unit	Schmid et al. 2008
Giudicarie Fault (GF) and Giudicarie Thrust Belt	Sinistral strike-slip fault; the related thrust belt emplaced upper Triassic carbonates (hangingwall) onto tilted upper Oligocene-lower Miocene limestone of the Brione Formation (footwall)		Castellarin et al. 2006, Luciani and Silvestrini 1996, Pomella et al. 2010, 2012
Helvetic Thrust Front (HV)	Helvetic Nappes	Subalpine Molasse	Burkhard 1986, Kempf and Pfiffner 2004, Pfiffner 2009
Mid-Hungarian Fault Zone (MH)	System of strike-slip faults juxtaposing the AlCaPa Mega-Unit (north) with the Tisza- and Dacia Mega-Units (south)		Fodor et al. 1998, Csontos and Nagymarosy 1998, Schmid et al. 2008
Penninic Front (PN)	Valais ophiolites (north) and Zone Houillère (south)	Units derived from the distal European margin	Ceriani et al. 2001, Loprieno et al. 2011
Periadriatic Fault System (PF)	Transpressive strike-slip fault system juxtaposes ductile part of Alps (north) with S-directed fold-and-thrust belts (south); continues eastward as the Balaton Fault (BA) beneath the Pannonian Basin		Schmid et al. 1989, Rosenberg 2004, Handy et al. 2005, Horváth et al. 2006
Piemont-Liguria Suture Front (PL)	Piemont-Liguria ophiolites (incl. Schistes Lustrés)	In Western and Central Alps: Units derived from the Briançonnais continental sliver; In Eastern Alps: European margin units (Helvetic & Ultrahelvetic Nappes above Subalpine Molasse, Venediger Nappe Complex in the Tauern Window) and the Folded Molasse (Subalpine Molasse)	Schmid et al. 2004

Table A1: Faults, tectonic units and sources used in the map reconstructions.

Faults used in reconstructions	Hangingwall units	Footwall units	References
Sava Suture Zone (SV)	European basement (Tisza & Dacia Mega-Units)	West Vardar ophiolites, Jadar-Kopaonik thrust sheet including Bükk Mts. Unit	Tomljenović et al. 2008, Schmid et al. 2008, Ustaszewski et al. 2010
Southern Alps Front (SA)	Basement slices and their Mesozoic cover in thrust sheets	Messinian sediments of the Po Plain and its subsurface	Pieri and Groppi 1981, Schönborn 1992, 1999, Schiunnach et al. 2010
Split-Karlovac Fault (SK)	Strike-slip fault crosscuting various units of the External Dinarides and containing narrow basins of early-middle Miocene lacustrine deposits		Chorowicz 1970, 1975, Schmid et al. 2008, de Leeuw et al. 2012
Subalpine Molasse Front (SM)	Subalpine Molasse	Plateau Molasse	Pfiffner 1986
Tisza-Dacia Front (TD)	Dacia Mega-Unit	Tisza Mega-Unit	Schmid et al. 2008
West Vardar Obduction Front (WV)	Composite nappes of the Internal Dinarides comprising imbricated West Vardar ophiolites and East Bosnia-Durmitor (Pelagonian) Unit	External Dinarides (Pre-Karst, High Karst, Budva-Krasta-Cukali and Kruja Units), Hellenides (Pindos and Cycladic blueschists)	Gawlick et al. 1999, Mandl 2000, Schmid et al. 2008, van Hinsbergen and Schmid 2012